A prefrontal cortex-lateral hypothalamus circuit controls stress-driven increased food intake

L.F. Supiot[1,2], K.L Kooij[1], W. Du[1], A.A.C. Benschop[1], A.S.J. Nicolson[1], R. Haak[1], I.G. Wolterink-Donselaar[1], M.C.M. Luijendijk[1], D. Riga[1,2], R.A.H Adan[1], R.B. Poorthuis[1*], F.J. Meye[1*]

1. Department of Translational Neuroscience, Brain Center, UMC Utrecht, Utrecht University, The Netherlands.

2. Department of Human Genetics, Center for Neurogenomics and Cognitive Research, Amsterdam University Medical Center, Amsterdam, The Netherlands.

*Equal contribution / corresponding author

Corresponding authors

Primary correspondence to Frank J. Meye: f.j.meye-2@umcutrecht.nl

Rogier Poorthuis: rogier.poorthuis@gmail.com

Abstract

Stress can drive overconsumption of high-fat foods. The medial prefrontal cortex (mPFC) is implicated in such stress-eating, but the underlying circuit mechanisms remain unclear. Here we show that mPFC projections to the lateral hypothalamus (LHA) are required for stress-induced fat intake in male mice. We find that mPFC-LHA stimulation in sated states increases fat intake. Social stress acutely engages mPFC-LHA neurons, and inhibiting this pathway selectively prevents stress-driven excess fat intake. Circuit mapping shows that mPFC neurons innervate GABAergic and glutamatergic LHA (LHA_{VGLUT2}) neurons, but that social stress preferentially engages mPFC-LHA_{VGLUT2} neurons and causes plasticity at mPFC-LHA_{VGLUT2} synapses. Specifically, stress weakens mPFC synapses onto LHA_{VGLUT2} neurons that curtail food intake, while strengthening mPFC synapses onto midbrain-projecting LHA_{VGLUT2} neurons linked to stress-eating. We show that LHA_{VGLUT2} neurons are required downstream mPFC targets for transforming stress into heightened fat intake. Overall, we identify the mPFC-LHA as a multi-branched network, indispensable for stress-eating.

Introduction

Stressful experiences drive excessive intake of rewarding foods rich in fat and/or sugar[1–3]. In vulnerable individuals, stress contributes to the development of obesity, or to the recurrent binge eating in Bulimia Nervosa (BN) and Binge Eating Disorder (BED)[4,5]. The prefrontal cortex (PFC), a stress-sensitive region important in decision making and strategy selection[6,7], is likely implicated in stress-driven food intake. In obese individuals and patients with BED/BN the PFC is hyperresponsive to food cues[8,9], and rodent studies have also demonstrated that stimulation of subsets of medial (m)PFC neurons can cause voracious food intake[3,10,11]. Despite its links to regulating eating behavior, it remains unknown whether the mPFC also transforms stressful experiences into excessive intake of palatable food, and if so through which network adaptations.

A likely downstream target of the mPFC is the lateral hypothalamic area (LHA). mPFC glutamatergic pyramidal neurons send direct projections to the LHA[12]. The LHA itself has a prominent role in food intake[13–16], and we recently showed that the LHA interacts with the ventral tegmental area (VTA) in the midbrain to drive stress-driven food intake[3]. Notably however, the LHA is highly heterogeneous in (functional) neuronal subtypes[3,14,15,17,18]. In particular, glutamatergic LHA neurons (LHA_{VGLUT2} cells) are commonly linked to curtailing food intake[15,17], although there are also glutamatergic LHA neuronal subtypes, including those that project to the VTA, that can promote food intake[3]. Furthermore, certain neuropeptidergic subsets of glutamatergic LHA neurons (e.g. orexin, MCH), as well as GABAergic LHA neurons (LHA_{VGAT} cells) can also promote food intake[15,17,19]. It is unclear which of these distinct LHA subtypes are innervated by mPFC, and how mPFC control, potentially over distinct LHA cell types, orchestrates (stress-driven) feeding responses.

We hypothesized that stress would alter mPFC control over LHA networks, by activating LHA neuronal sets linked to promoting food intake, and/or by inhibiting neuronal sets linked to curtailing feeding, to causally drive excessive palatable food intake. Here we show, in mice, that optogenetic stimulation of the mPFC-LHA pathway is capable of driving intake of fat over chow.

We use *in vivo* electrophysiology and fiber photometry to demonstrate that mPFC cells projecting to the LHA are directly sensitive to social stress and are engaged during fat intake. We demonstrate that mPFC-LHA pathway activity, while not important for regular feeding, becomes indispensable for the hyperphagia occurring after social stress. We investigated the downstream targets of mPFC, by combining patch clamp and optogenetics, showing that mPFC cells make direct synapses onto multiple LHA cellular subtypes. In the aftermath of stress, when the drive for food intake is increased, we observe weakening of mPFC glutamatergic synapses onto LHA_{VGLUT2} cell types linked to reducing food intake but strengthening of mPFC inputs onto LHA_{VGLUT2}-VTA cells, which we previously implicated in mediating stress-driven binge responses[3]. Using *in vivo* optogenetics we show that these divergent stress-driven circuit modifications increase the efficacy with which the mPFC-LHA network can persistently drive fat intake. Finally, we use circuit and neuronal ensemble-based approaches to identify that LHA_{VGLUT2} neurons, downstream of the mPFC, are indispensable integrators of stress information and subsequent hyperphagia. Overall, we identify the mPFC as a direct regulator of multiple LHA feeding networks, with a critical role of this network in stress-driven excess intake of palatable fat.

Results

mPFC-LHA stimulation, in a frequency-dependent manner, increases palatable food intake

We first assessed whether the mPFC-LHA pathway is capable of driving intake of palatable food, as thus far this had not been reported. Instead, prior studies evaluating the mPFC-LHA pathway showed that high frequency optogenetic stimulation (100Hz bursts) does not affect regular food intake[20], while continuous chemogenetic stimulation (or 20Hz optogenetic stimulation) decreases chow intake[21]. Notably, neural circuits of mPFC and LHA are individually known to have frequency-dependent functions, with lower frequency stimulation able to drive distinct behaviors[19,22]. Therefore, we tested whether low frequency stimulation of the mPFC-LHA pathway can increase palatable food intake. We stereotactically injected C57B6 mice in the mPFC with an AAV to express the optogenetic construct CoChR (rAAV5-Syn-CoChR-GFP) or YFP

89 control vector (rAAV5-Syn-eYFP), and targeted optic fibers to the LHA to optogenetically
90 stimulate the mPFC-LHA pathway (Fig 1A-B; Suppl Fig. 1A). After recovery, mice were placed in a
91 2-choice food-context containing regular chow and fat as a palatable food source. Baseline food
92 intake was established over 3 consecutive days, followed by a session during which the mPFC-
93 LHA pathway was stimulated at a specific frequency (Fig. 1C). We observed that during sessions
94 of 5Hz stimulation, but not of 1 or 10Hz, there was an overall increase of fat intake (Fig. 1D;
95 Suppl Fig. 1B). Between the two choices, this increased intake was specific to fat, as it did not
96 occur for chow (Suppl Fig. 1C).

97 We then used video-based analysis to examine the feeding behavior within mPFC-LHA
98 stimulation blocks (ON), contrasting them with behavior during alternating non-stimulated
99 blocks (OFF). We observed that with 5Hz stimulation mice spent more time in specifically the fat
100 zone (Suppl. Fig. 1D). Furthermore, we observed that the effect of pathway stimulation on fat
101 consumption differed over the course of the task. Interactions with fat normally waned over the
102 hour (Fig. 1E). Whereas 5Hz stimulation of the pathway did not affect fat intake at the start,
103 when the drive for fat was still high, it instead drove continued fat consumption later on when
104 such interactions had typically waned, as seen in the control groups and in the 1Hz stimulation
105 conditions (Fig. 1E). Consequently, 5Hz stimulation resulted in overall more feeding bouts for
106 fat, but not chow (Fig. 1F; Suppl. Fig. 1E). These effects on food intake did not stem from effects
107 of pathway stimulation on general locomotor activity, which increased linearly in a different
108 pattern from the effect on food intake (Suppl. Fig. 1F), nor did they stem from any direct
109 alterations of emotional valence states, as assessed with a real-time place
110 preference/avoidance assay (Suppl. Fig. 1G). Overall, these data indicate that the mPFC-LHA
111 pathway is able, at least in the lower frequency domain, to drive the continued intake of
112 palatable fat.

113

114 **mPFC cells projecting to LHA modulate their firing in response to social stress**

115 Stressful experiences can drive excessive food intake (i.e. hyperphagia)[3,23], ultimately causing
116 weight gain[23]. We reasoned that if the mPFC-LHA network would be involved in stress-driven
117 effects on food intake, that it should be able to detect stressful information. To test this

118 hypothesis, we used a social stress experience, where a mouse is temporarily exposed to the
119 aggression and proximity of a dominant conspecific. We and others have previously shown that
120 hours to days after such social stress there is an increased intake of high palatable foods such as
121 fat[3,23].

122 We assessed whether social stress would immediately engage the mPFC-LHA pathway. To this
123 end we performed *in vivo* electrophysiological recordings from mPFC cells projecting to the LHA.
124 We injected, in C57B6 mice, a canine adeno virus in the LHA to retrogradely deliver Cre (Cav2-
125 Cre) to the mPFC, and an AAV in the mPFC to Cre-dependently drive an opsin (AAV-DIO-
126 hChR2(H134R)-mCherry). We then chronically implanted electrodes together with an optic fiber
127 (i.e. an optrode) in the mPFC of these mice (Fig. 2A-B). This allowed for optogenetic-assisted
128 identification (i.e. opto-tagging) of mPFC cells that projected to the LHA (Fig. 2C; Suppl. Fig. 2A-
129 B). We then exposed these mice to the sensory proximity of a CD1 mouse and the actual fight
130 experience with such an aggressor, while performing single cell recordings from opto-tagged
131 mPFC-LHA cells (Fig. 2D). We analysed firing rates of opto-tagged neurons before, during and
132 after the period in which fighting took place. Divergent responses were observed in mPFC
133 neurons projecting to LHA during stress, with approximately half of the cells decreasing their
134 firing rates during fight periods, whereas others instead were not affected or showed increased
135 firing rates (Fig. 2E-F). These effects were not solely linked to the physical altercation, as they
136 outlasted the fighting period (Fig. 2E; Suppl. Fig. 2C-D). In further support of this, we also
137 evaluated the responses of these same neurons when the CD1 mouse arrived in the cage, while
138 still behind a semi-permeable barrier (i.e. sensory stress). We observed similar response types,
139 where in particular the neurons that increased their firing during sensory stress, were
140 modulated in the same direction during physical exposure (Suppl. Fig. 2E-H). Aside from
141 evaluating opto-tagged mPFC neurons with confirmed projections to the LHA, we also evaluated
142 putative pyramidal mPFC neurons that were not opto-tagged. Such neurons responded with
143 excitations or inhibitions to social stress (Suppl. Fig. 2I-J), although they were less often
144 modulated by stress than the mPFC-LHA population (Suppl. Fig. 2I). Overall, these data indicate
145 the existence of different populations of mPFC-LHA neurons, with certain mPFC-LHA neurons
146 acutely decreasing their activity, and others directly increasing it upon social stress exposure.

147 These findings confirm the hypothesis that mPFC cells that project to LHA are directly able to
148 detect a social stressor with known hyperphagic properties [3,23].

149

150 **mPFC-LHA pathway activity is indispensable for stress-driven excess fat intake**

151 We showed that activity of the mPFC-LHA pathway is modulated by a social stressor. Next, we
152 asked whether activity in this pathway is necessary for stress-driven increases in food intake. To
153 this end we bilaterally expressed an inhibitory chemogenetic receptor in the mPFC-LHA pathway
154 in C57B6 mice. Specifically, we stereotactically injected Cav2-Cre retrograde virus in the LHA,
155 and an AAV to Cre-dependently drive hM4Di (or a control fluorophore) in the mPFC (Fig. 3A-B).
156 We confirmed that this indeed resulted in chemogenetic control over LHA-projecting mPFC
157 cells. In brain slices we patch-clamped such mPFC neurons and found that bath administration
158 of DREADD agonist CNO resulted in strong hyperpolarization of the neurons (Suppl. Fig. 3A).

159 We then tested whether chemogenetic inhibition of the pathway would alter regular or stress-
160 driven feeding behavior. We again placed animals in the 2-choice model (as in Fig. 1C) during a
161 baseline session. Then we exposed the mice to either two days of social stress (which we
162 previously showed to increase fat intake[3]) or to control exposure. The next day we systemically
163 administered CNO to the animals, and 45 minutes later reintroduced them to the 2-choice
164 model (Fig. 3C). Mice with control mCherry vectors in the mPFC-LHA pathway exhibited clear
165 stress-driven increased intake compared to their baseline. In mice with hM4Di in their mPFC-
166 LHA pathway, we observed that inhibiting the pathway had no effect on food intake for non-
167 stressed mice. Instead, in stressed-mice it completely counteracted the amount of
168 overconsumption that occurred after stress (Fig. 3C-D, Suppl. Fig. 3B). The effects of mPFC-LHA
169 pathway inhibition were not due to actions on locomotor behavior or altered anxiety (Suppl. Fig.
170 3C-D). No differences were observed for chow intake (Fig. 3D). Overall, this suggests that mPFC-
171 LHA pathway activity is not required for regular food intake, but becomes indispensable for
172 regulating the excess food intake after stress.

173

174 **mPFC neurons projecting to LHA respond to food intake**

175 We next investigated whether the mPFC-LHA pathway would be responsive to food intake, and
176 stress-modulations thereof. We investigated the mPFC-LHA pathway in this case by measuring
177 population-level calcium responses using fiber photometry. We stereotactically injected Cav2-
178 Cre in the LHA, injected an AAV for Cre-dependent expression of calcium indicator GCaMP8s in
179 the mPFC, and placed a fiber for photometric measurements above it (Fig. 3E; Suppl. Fig. 3G).
180 We first validated that we could measure from this pathway. Our in vivo electrophysiology data
181 had shown that social stress is a modulating experience for this pathway, resulting at the single
182 cell level at either excitation or inhibition in a considerable subset of cells (Fig. 2E-F). When we
183 exposed mice to the social aggression of a CD1 mouse, we observed a biphasic calcium response
184 of the mPFC-LHA at population level to this stimulus, with a peak, and a subsequent dip in
185 calcium responses (Fig. 3F-G; Suppl. Fig. 3H). This confirms that with fiber photometric
186 measurements we can pick up relevant dynamics in this pathway.
187 We then evaluated the response of the mPFC-LHA pathway to food intake. For that we placed
188 animals in the 2-choice task with access to fat and chow. We observed that when mice ate, and
189 particularly when they ate fat, there were pronounced dips in calcium signals recorded from
190 mPFC neurons projecting to LHA (Suppl. Fig 3I). These were time-locked to the onset of food
191 contact and waned after disengagement from the food source (Suppl. Fig. 3I). We then
192 evaluated whether such responses, measured from mPFC somata, would be altered by prior
193 stress. We exposed the mice again to a two-day social stress paradigm (or to control). We then
194 recorded the day after, where normally there would be an increased food intake (Fig. 3D).
195 However, we observed the same type of feeding-related dip responses in the pathway in control
196 and in stressed mice (Fig. 3H-J). Hence, although the mPFC-LHA pathway is modulated during
197 both stress and during feeding responses, and stress alters feeding responses, we did not
198 observe signs of stress-driven plasticity in LHA-projecting mPFC soma reactivity during stress-
199 driven hyperphagia. We next investigated whether stress-driven plasticity would instead occur
200 at downstream mPFC synapses onto LHA neurons.
201
202 **mPFC neurons make monosynaptic connections to multiple types of LHA neurons.**

203 Our findings demonstrate that the mPFC neurons projecting to the LHA respond to social stress
204 and are capable of altering food intake, respond to food intake, and subsequently are necessary
205 for stress-driven over consumption of fat. However, no changes were observed in somatic
206 population activity of mPFC-LHA cells after stress while interacting with palatable food. This led
207 us to hypothesize that plasticity of downstream communication with different populations in
208 the LHA might underlie alterations in fat intake. However, it is unclear which LHA neuronal
209 subtypes are innervated by the mPFC. The LHA contains both glutamatergic populations,
210 expressing the vesicular glutamate transporter 2 (LHA_{VGLUT2}) and GABAergic populations,
211 identified by expression of the vesicular GABA transporter (LHA_{VGAT}). Recent transcriptomic
212 evidence suggests that essentially all LHA neurons can be ascribed to one of these major classes,
213 with further key subpopulations occurring within them[15,18]. For instance, evidence suggests that
214 orexin (LHA_{OREX}) and melanin-concentrating hormone (LHA_{MCH}) releasing neurons represent
215 distinct subsets of LHA glutamatergic (VGLUT2+) neurons, but also that most LHA_{VGLUT2} neurons
216 do not belong to those specific subsets[18]. We reasoned that, despite further heterogeneity within
217 LHA_{VGAT}, LHA_{VGLUT2}, LHA_{MCH} and LHA_{OREX} neuronal sets[15,18], these four populations offer a starting
218 point to understand mPFC functional innervation patterns of the LHA.

219 To map mPFC connectivity to these four LHA subpopulations we performed an optogenetic-
220 assisted synaptic connectivity study[24,25]. We targeted the mPFC with the opsin CoChR (AAV5-
221 Syn-CoChR-GFP) and fluorescently labeled LHA_{VGLUT2}, LHA_{VGAT}, LHA_{MCH} or LHA_{OREX} populations
222 with viral and transgenic strategies. For LHA_{VGLUT2} and LHA_{VGAT}, populations we used well-
223 established transgenic mice VGLUT2-Cre or VGAT-Cre mice, respectively (Fig. 4A-B). We injected
224 these mice in the LHA with an AAV to Cre-dependently express a red fluorophore (rAAV-EF1a-
225 DIO-mCherry) to label either LHA_{VGLUT2} or LHA_{VGAT} neurons, respectively (Fig. 4A-B). Instead to
226 target LHA_{OREX} or LHA_{MCH} neurons we injected C57B6J mice with an AAV to drive expression of a
227 red fluorophore under the control of short promotors for either MCH (AAV-MCHpr-Gq-mCherry)
228 or orexin (AAV-hORXpr-TdTomato)[26] (Fig. 4A-B). We established the specificity of this approach
229 using post-hoc labeling of biocytin-filled patched cells expressing either the fluorophore under
230 control of the orexin or the MCH promotor (Suppl. Fig. 4A-C). We also established that the
231 LHA_{VGLUT2} cells that we on average targeted were distinct from the LHA_{OREX} and LHA_{MCH} cells, as

232 those peptidergic subpopulations of glutamatergic neurons differed strongly in somatic cell size
233 from typical LHA_{VGLUT2} neurons (Suppl. Fig. 4D). The four distinct LHA populations also differed
234 from each other in other biophysical properties further corroborating that different LHA
235 populations were sampled from (Suppl. Fig. 4E-I). We also established that both LHA_{VGAT} and
236 LHA_{VGLUT2} neurons were able to follow protracted optogenetic stimulation of mPFC inputs at
237 least for 1 and 5 Hz, whereas for 10 Hz fidelity of induced postsynaptic potentials remained
238 higher onto LHA glutamatergic neurons (Suppl. Fig. 4J).

239 We then performed *ex vivo* patch clamp recordings to assess the occurrence of mPFC synaptic
240 inputs onto these LHA subpopulations. We observed high degrees (≥80%) of connectivity
241 between mPFC cells and all four LHA populations (Fig. 4C). We then repeated these experiments
242 in the presence of a pharmacological cocktail of tetrodotoxin (TTX) and 4-aminopyridine (4-AP)
243 in the external medium[24,27] and confirmed that the high extent of connectivity of mPFC inputs
244 with all LHA subtypes was due to direct monosynaptic connections (Fig. 4D). Together these
245 data indicate that there is a strong monosynaptic projection from the mPFC cells to all four LHA
246 subpopulations.

247

248 **Stress selectively affects mPFC synaptic contacts onto LHA_{VGLUT2} neuronal populations via**
249 **presynaptic processes.**

250 After social stress there is an increased drive for the intake of palatable food sources rich in
251 sugar and fat[3,23], which ultimately results in excess body weight if maintained over weeks[23]. In
252 the fiber photometric experiment, we observed that at the level of mPFC cell bodies the two-
253 day stress model did not affect response magnitudes. However, it remains possible that
254 downstream, at the synaptic level, changes occurred due to stress. We therefore next asked if,
255 at the time of stress-driven hyperphagia, mPFC synaptic strength onto distinct LHA neuronal
256 populations would be altered. To address this, we evaluated the effects of stress on mPFC
257 synaptic contacts onto the four distinct LHA populations (LHA_{VGLUT2}, LHA_{VGAT}, LHA_{MCH}, LHA_{OREX}).
258 We expressed an opsin in the mPFC (AAV-CoChR-GFP) and tagged distinct LHA populations as
259 before (Fig. 4A-B; Suppl. Fig. 5A-B). We exposed mice to two days of control experience or social

260 stress, and then the next day, when mice normally engage in higher intake of palatable food[3]
261 (Fig. 3D) we made brain slices and assessed synaptic properties at mPFC synapses onto the four
262 broad classes of LHA neuronal populations (Suppl. Fig. 5A-C).
263 Interestingly, we observed that specifically at the mPFC synapses onto LHA_{VGLUT2} neurons there
264 was on average a stress-induced decrease in maximally optogenetically-evoked EPSC
265 magnitudes (Fig. 5A; Suppl. Fig. 5C). This suggests a weakening of glutamatergic mPFC synapses
266 onto many LHA_{VGLUT2} neurons. To further address the underlying mechanisms for this we
267 assessed the paired pulse ratio (PPR), a measure inversely related to presynaptic release
268 probability[24]. We observed that specifically at mPFC- LHA_{VGLUT2} synapses there was an increased
269 PPR, in accordance with a scenario of lower release probability at these synapses due to prior
270 social stress (Fig. 5B; Suppl. Fig. 5D). The effect of stress was specific to the presynaptic
271 compartment, as we did not observe a difference in postsynaptic glutamatergic receptor
272 distributions at these synapses (Suppl. Fig. 5E). Nor did we observe changes due to stress in
273 terms of the excitability of the LHA cells or in basic membrane properties (Suppl. Fig. 5F-G).
274 These data suggest that social stress alters mPFC glutamatergic synapses onto LHA_{VGLUT2}
275 neurons. We next asked whether another stressor would similarly be able to induce these
276 effects. For another stress experience of a different modality, we exposed mice to restraint
277 stress (Suppl. Fig. 6A), and we observed that this also subsequently increased intake of fat
278 (Suppl. Fig. 6B). Similarly to social defeat stress, restraint stress also reduced the magnitude of
279 mPFC synaptic responses onto LHA_{VLUT2} neurons (Suppl. Fig. 6C-D), and it also increased the PPR
280 at these synapses, indicating a similar mechanism of reduced release probability between the
281 different types of stressors (Suppl. Fig. 6E). Overall, these data suggest that after stressful
282 experiences, which can drive binge intake of fat, there is on average a weakening of mPFC
283 glutamatergic synapses onto the global population of LHA_{VGLUT2} neurons, which on average
284 reduces food intake upon activation[15,17].
285
286 **Social stress has divergent effects on distinct populations of mPFC-innervated LHA_{VGLUT2} cells**
287 LHA_{VGLUT2} neurons still represent a very heterogeneous population[18] and in part this
288 heterogeneity is reflected by their distinct projection targets[28]. For instance, stimulating

289 LHA_{VGLUT2} projections to the lateral habenula (LHb) suppresses food intake[29]. Similarly
290 stimulating LHA_{VGLUT2} neuronal projections to midline hypothalamic regions around the third
291 ventricle (i.e. peri-paraventricular nucleus, or peri-PVN region[30]) is linked to aversive processes[31]
292 and reduced food intake[32]. Instead LHA_{VGLUT2} projections to the ventral tegmental area (VTA) do
293 not alter food intake under naïve conditions[3,33,34], but the potentiation of their synapses onto
294 dopamine neurons causally contributes to the enhanced fat intake occurring after social stress[3].
295 Given this LHA_{VGLUT2} anatomical but also functional divergence, we therefore asked how social
296 stress would affect mPFC synapses onto such distinct LHA_{VGLUT2} populations. We first assessed
297 that the LHb, VTA and (peri)-PVN could be downstream targets of mPFC-innervated LHA
298 neurons. For this we used a transsynaptic tracing strategy (Suppl. Fig. 6F) in which we injected
299 AAV1-Cre in the mPFC, to cause a transsynaptic jump to downstream neurons[35]. We then
300 injected an AAV-DIO-GFP in the LHA to perform anterograde tracing of the nerve terminals
301 belonging to LHA neurons with mPFC-innervation (Suppl. Fig. 6F-G). We indeed observed
302 anterograde terminals in the regions of interest like the VTA, the LHb and the peri-PVN (Suppl.
303 Fig. 6H).
304 We then investigated if and what type of stress-driven synaptic changes occurred at mPFC
305 synapses onto LHA_{VGLUT2} neurons projecting to LHb, VTA and peri-PVN. To label LHA_{VGLUT2} cell
306 types based on their projection output, we injected a Cre-dependent retrograde tracer
307 (retroAAV-DIO-mCherry) in Vglut2-Cre mice in these three different areas (Fig. 5C-D). We then
308 again exposed mice to either two days of control or social stress conditions and we prepared
309 brain slices the day after and patched from retrogradely traced LHA_{VGLUT2} neurons, assessing
310 their mPFC input (Fig. 5C). We observed that mPFC synapses onto LHA_{VGLUT2}-Peri-PVN neurons
311 exhibited higher PPR upon stress (Fig. 5E), in accordance with the general effect of stress on the
312 LHA_{VGLUT2} neurons (Fig. 5B). We confirmed, via in vivo optogenetic stimulation of the LHA_{VGLUT2}
313 projection to the peri-PVN, that this pathway indeed reduces food intake upon activity (Suppl.
314 Fig.6K-M) as previously suggested[32]. In contrast to the effect of stress on mPFC-LHA_{VGLUT2}-Peri-
315 PVN synapses, we instead did not observe PPR changes at mPFC synapses onto LHA_{VGLUT2}-LHb
316 neurons after stress (Fig. 5F). Interestingly, we observed that mPFC synapses onto LHA_{VGLUT2}-
317 VTA neurons presented a lower PPR after stress, suggesting enhanced release probability of

318 mPFC synapses onto those specific LHA_{VGLUT2} neurons (Fig. 5G). In accordance, we had
319 previously shown that stress-driven strengthening of LHA glutamatergic synapses onto VTA
320 dopamine neurons is linked to stress-driven fat intake[3].
321 Overall, these data suggest that social stress has divergent effects on the strength of mPFC
322 synapses onto distinct LHA_{VGLUT2} populations. On the one hand weakening excitatory mPFC
323 synapses onto LHA_{VGLUT2} populations with a role in braking food intake[32], whereas on the other
324 hand strengthening excitatory PFC synapses onto LHA_{VGLUT2} populations with a role in promoting
325 food intake under stress[3].
326
327 **After social stress mPFC-LHA activity is more primed to drive feeding.**
328 We reasoned that the consequences of such stress-driven network modifications could prime
329 the mPFC-LHA pathway to become even more capable of driving palatable food intake when
330 stimulated.

331 To test this, we again optogenetically probed the mPFC-LHA pathway, by stereotactically
332 injecting C57B6J mice with an optogenetic construct (rAAV5-Syn-CoChR-GFP) and implanting
333 optic fibers bilaterally above the LHA (Fig. 6A-B). After recovery we either exposed the mice to
334 two days of social stress or housed them with a novel cage mate. Subsequently we placed the
335 animals in a limited access food choice setting, where they could consume fat or chow for 2
336 hours. Mice were again exposed to recurring blocks of optogenetic stimulation of 5Hz, or
337 instead to mock stimulation (Fig. 6A). We observed that even though mice that had previously
338 experienced stress already consumed more fat than control mice, optogenetic stimulation could
339 drive their intake of palatable food even further, making these mice the largest consumers of fat
340 (Fig. 6C), in the absence of effects on chow (Suppl. Fig. 7A).

341 The overall fat intake reflected the outcome at the end of the two-hour binge period. We next
342 addressed, with more fine-grained temporal resolution, whether optogenetic stimulation was
343 more efficient in driving fat intake in stressed mice as compared to control mice. We first aimed
344 to better understand the development of fat intake under stress (without pathway stimulation).
345 We observed that regular (not stimulated) stressed animals performed over 75% of their fat
346 feeding bouts in the first 20 minutes of a session, and then strongly diminished interaction with

347 the fat from thereon (Fig. 6D-E). This binge-like feeding pattern of fat for stressed mice was
348 different from control mice, which had fewer immediate feeding bouts, but continued having
349 feeding bouts for a longer period (Fig. 6D-E). We then analyzed how in these two distinct phases
350 that we refer to as "Binge Phase" (i.e. 0-20 min) and "Post-Binge phase" (20-120 min), mPFC-
351 LHA pathway stimulation affected fat interaction. Reminiscent of our previous finding of
352 pathway stimulation early in the 2-choice session in naïve mice (Fig. 1E), we found that 5Hz
353 mPFC-LHA stimulation was not effective in the early "Binge Phase" of the session (Fig. 6F).
354 Instead in the subsequent "Post Binge" phase 5Hz stimulation particularly drove stressed mice
355 more potently towards the fat, when they would normally be in more sated conditions (Fig. 6F).
356 To investigate whether indeed the 5Hz stimulation could prevent a decline of interest for the
357 fat, we plotted the relative drive for fat eating over the course of the task by comparing the
358 relative amount of feeding bouts taking place during the binge and post-binge period. Indeed,
359 particularly in stressed mice, 5Hz stimulation did not affect the binge intake, but it did
360 counteract the normally occurring decline of interest in the fat later on (Fig. 6G). Overall, these
361 data reveal that after stress mPFC-LHA network activity is primed more towards an ability to
362 drive fat intake.

363

364 **A role for glutamatergic LHA neurons in transferring effects of stress into binge of fat**

365 We further sought to investigate the importance of LHA neuronal subsets downstream of the
366 mPFC in mediating stress-driven feeding. Glutamatergic LHA neurons are an interesting
367 candidate. It is on this subset that we observed stress-driven plasticity of mPFC synaptic inputs
368 (Fig. 5A-B). Moreover, LHA_{VGLUT2} neurons show strong increased calcium reactivity during social
369 stress[3]. We first asked whether inhibiting the activity of LHA_{VGLUT2} neurons during social stress
370 would prevent subsequent binge eating. To test this, we injected a Cre-dependent inhibitory
371 DREADD (AAV-DIO-hM4Di-mcherry) in the LHA of Vglut2-Cre mice (Fig. 7A-B). We subsequently
372 subjected the mice to either the two-day social stress paradigm or its control. Prior to such
373 stress (or control) events we administered either vehicle or CNO. Chow intake in general was
374 minimal and unaffected (not shown). Importantly however, we observed that inhibition of

375 LHA_{VGLUT2} neurons during social stress episodes fully blocked subsequent binge eating of fat (Fig.
376 7C). Indicating that these neurons are important for the induction of stress-eating.

377 We next evaluated whether activity of LHA_{VGLUT2} neurons could also contribute to the effects of
378 optogenetic stimulation of the mPFC-LHA pathway on food intake. In Vglut2-Cre mice, we
379 injected AAV-hSyn-CoChR-GFP in the mPFC and placed optic fibers in the LHA for pathway
380 stimulation. We also injected an AAV-DIO-hM4Di-mCherry in the LHA to be able to
381 chemogenetically inhibit LHA_{VGLUT2} neurons (Suppl. Fig. 7B-C). We then assessed food intake
382 during a baseline period in the mice in the 2-choice paradigm (Fig. 1C). After baseline periods
383 we, in randomized order, re-exposed mice to the 2-choice paradigm during one of four
384 conditions: optogenetic stimulation of the mPFC-LHA pathway or not, with chemogenetic
385 inhibition of LHA_{VGLUT2} neurons (CNO administration prior to the test) or not. When we did not
386 inhibit LHA_{VGLUT2} neurons we again observed an increase in fat intake in response to pathway
387 stimulation (Suppl. Fig. 7D). Chemogenetic inhibition of LHA_{VGLUT2} neurons (without stimulation)
388 also gave a trend towards increased food intake. If the sole role of LHA_{VGLUT2} neurons would be
389 to inhibit food intake, then mPFC-LHA stimulation without LHA_{VGLUT2} contributions (i.e. mainly
390 then favoring mPFC-innervated LHA_{VGAT} recruitment) should make mPFC-LHA stimulation even
391 more potent in driving food intake. Instead, we observed that optogenetic stimulation of the
392 mPFC-LHA pathway during LHA_{VGLUT2} inhibition did not significantly further increase the intake
393 of fat beyond LHA_{VGLUT2} inhibition itself (Suppl. Fig. 7D). This did not appear to be due to a time-
394 constraint limit on feeding, as overnight food deprived animals still consumed considerably
395 more as a control (Suppl. Fig. 7D).

396 Together these results suggest that activity of LHA_{VGLUT2} neurons during stress is required for
397 subsequent excess food intake, and it also suggests that despite many LHA_{VGLUT2} neurons
398 curtailing food intake, the activity of at least some LHA_{VGLUT2} subsets also participates in the
399 mPFC-LHA pathway ability to drive food intake upon stimulation.

400

401 **Stress-sensitive mPFC neurons project to glutamatergic LHA neurons and can drive increased**
402 **intake of fat**

403 We then also employed another strategy to try to parse out the most relevant branches in the
404 mPFC-LHA network involved in stress-driven food intake. For this we used an activity-dependent
405 genetic labeling approach and investigated the neurons in the mPFC-LHA axis sensitive to stress,
406 to determine their role in feeding. We expressed an optogenetic construct in those mPFC cells
407 that were reactive during the social stress (as opposed to all mPFC neurons). For this we used
408 TRAP2 (Targeted Recombination in Active Populations) transgenic mice, in which the immediate
409 early gene c-Fos can drive Cre-ERT2 expression, which can then be conditionally transported
410 from the cytosol to the nucleus in a manner dependent on 4-OH tamoxifen[36]. We previously
411 showed that this strategy can be leveraged to capture social stress-reactive neuronal
412 ensembles[37]. We crossed these TRAP2 transgenic mice with either VGAT-Cre or VGLUT2-Cre
413 mice and used the resultant offspring. We first injected an AAV driving Cre-dependent CoChR in
414 the mPFC and exposed the mice to two stress episodes, where each episode was paired with a
415 4-OH tamoxifen injection. Weeks later we also injected AAVs in the LHA to fluorescently label
416 specific subpopulations such as $LHA_{VGLUT2,}$ LHA_{VGAT}, LHA_{OREX} and LHA_{MCH} cells as before (Fig. 7D-F;
417 Suppl. Fig. 7B-C). Importantly, while both TRAP2 transgenic mice, and VGAT-Cre / VGLUT2-Cre
418 transgenic mice, rely on conditional expression via the same Cre-LoxP system, the viral injection
419 scheme in this case avoided interference between this. First, we avoided mPFC CoChR
420 expression in a manner not linked to the TRAPing of an ensemble in the VGLUT2-Cre mice, on
421 the basis of mPFC neurons expressing VGLUT1 rather than VGLUT2[21,38] (Suppl. Fig. 7E). We also
422 avoided that there would be Cre-dependent fluorophore recombination in the LHA driven by
423 the TRAP system rather than on the basis of LHA cell type identity, by performing the LHA viral
424 injection several weeks after the 4OH-tamoxifen dependent TRAPing event in the mPFC had
425 taken place (Fig. 7D), whereas the time window in which 4OHT allows Cre to travel to the
426 nucleus for recombination is only a matter of hours[36,37]. Finally, we also took along a control
427 ensemble of exposure to a novel mouse rather than stressful altercations (Fig. 7D). In both the
428 social stress TRAP experiment and the novel mouse TRAP experiment we observed expression
429 of CoChR in mPFC ensembles (Fig. 7E; Suppl. Fig. 7F). We then performed patch-clamp
430 recordings in the LHA and assessed whether optogenetic stimulation of $mPFC_{NOVEL\ MOUSE}$ or
431 $mPFC_{SOCIAL\ STRESS}$ ensembles resulted in synaptic contacts with specific LHA cell types. Stimulating

432 the $mPFC_{NOVEL\ MOUSE}$ ensemble caused relatively little connectivity with the LHA, though there
433 was connectivity with LHA_{MCH} neurons (Fig. 7G-H). In contrast, optogenetically stimulating the
434 $mPFC_{SOCIAL\ STRESS}$ ensemble resulted in synaptic responses in LHA_{VGLUT2}, LHA_{MCH}, and LHA_{OREX}
435 neuronal subsets (Fig. 7G-H). Instead, LHA_{VGAT} neurons received almost no input (Fig. 7G-H).

436 These results suggest that mPFC neurons that are modulated within the time window of several
437 hours during social stress experiences send preferential projections to glutamatergic neurons
438 (including its peptidergic subtypes[18]) over GABAergic LHA neurons. Given that we had shown
439 the importance of glutamatergic LHA neurons in mediating the effects of stress on food intake
440 (Fig. 7C), we next asked whether optogenetically stimulating $mPFC_{SOCIAL\ STRESS}$ projections to
441 these glutamatergic LHA neurons would modulate food intake. We used TRAP2 mice in which
442 we again expressed an optogenetic construct (AAV-DIO-CoChR-GFP) in the mPFC, placed an
443 optic fiber in the LHA, and triggered recombination of the opsin in the mPFC either by pairing
444 the social stress experiences or the novel mouse experiences with 4OH-tamoxifen injections
445 (Fig. 7I-J). After recovery we optogenetically stimulated these pathways with 5Hz in the context
446 of the 2-choice food assay. We observed that optogenetic stimulation of the $mPFC_{SOCIAL\ STRESS}$ to
447 LHA pathway resulted in increased fat intake (Fig. 7K), without altering chow intake (Suppl. Fig.
448 7G). Together these results suggest that glutamatergic LHA neurons are important downstream
449 targets of the mPFC for the effects of stress on increased food intake.

450

451 **Discussion**

452 Uncovering the neurobiological substrate for stress-driven overconsumption of palatable foods
453 is an important topic, also in view of the contributions of such behavior to eating disorders like
454 Binge Eating Disorder and Bulimia Nervosa, and to obesity[2,39]. The prefrontal cortex is
455 implicated in binge eating disorders[9], but it has been unclear through which network
456 adaptations it could orchestrate stress-driven food intake. Here we show that there is direct
457 mPFC control over distinct LHA circuits, and that stress-driven alterations of the mPFC-LHA
458 network contribute to overconsumption of palatable fat. Here we discuss multiple facets of
459 these findings.

460

461 <u>The mPFC-LHA pathway has a conditional role in food intake driving excess intake</u>

462 Our pathway stimulation and inhibition experiments reveal that the mPFC-LHA network plays a
463 conditional role in food intake. Firstly, the role of the pathway in feeding was only unmasked by
464 stress. Chemogenetic inhibition of the pathway under normal (non-stressed) conditions did not
465 alter food intake, in accordance with an earlier study[21]. Instead, we show that after a social
466 stress experience that drives excess intake of specifically palatable food[3], inhibition of the
467 pathway abolished not all feeding, but rather only the amount of excess fat intake due to stress.
468 This suggests that the pathway is not generally necessary for feeding behavior, but its
469 importance emerges under certain conditions like a stressed state.

470 Secondly, mPFC-LHA pathway stimulation increased the intake of palatable fat, without
471 affecting concurrently available chow. This indicates that the circuit manipulations caused a
472 directed increased drive towards palatable foods, rather than an indiscriminate urge to chew.
473 Although not explicitly tested here, we consider it likely that the stress-driven effects mediated
474 by the mPFC-LHA network results in an increased preference for palatable food in general,
475 rather than a nutrient-specific preference for fat. In support of this, moderate social stress
476 causes preference for palatable food in general, including both fat and sucrose[3]. Thirdly, our
477 data suggest that internal states may contribute to the role of mPFC-LHA pathway in food
478 intake. We observed that the optogenetic stimulation of the pathway did not cause altered food
479 intake at the start of feeding sessions, when the drive for food intake was still high. Instead, it

480 was only at later timepoints, when normally food interest would have waned, that pathway
481 stimulation caused continued food interest and time spent eating. This finding also indicates
482 that the role of mPFC-LHA networks will likely depend on whether or not animals are food
483 deprived. In our pathway manipulation experiments animals were ad libitum-fed, perhaps
484 allowing disinterest in food to occur more quickly under normal circumstances, and revealing a
485 role for mPFC-LHA network activity more readily.
486 Our fiber photometric data show that the mPFC-LHA pathway shows a transient decrease in
487 activity during food intake, which reverses upon the end of contact with the food, in accordance
488 with a previous study[21]. It is of note that increasing mPFC-LHA pathway activity, at least at
489 certain frequencies, drives food intake, whereas mPFC-LHA pathway activity decreases during
490 the actual food intake. It is interesting to compare this with systems with a link to feeding. For
491 instance, arcuate nucleus AgRP neurons are potent drivers of food intake when stimulated yet
492 also show dips in their activity during food intake. This may reflect an encoded energy need
493 signal of these neurons that is then attenuated during caloric intake[40–43]. Somewhat
494 analogously, mPFC-LHA pathway activity may reflect not a generic energy deficit signal, but
495 more a conditional one, promoting further intake of palatable energy-dense foods, emerging
496 under specific circumstances, such as after stress. Another interpretation is that mPFC-LHA
497 pathway activity reflects an engagement signal to continue to seek out palatable food instead of
498 moving on to other activities. Actual consumption of the food may then require a brief decrease
499 in such activity to allow for consumption instead of seeking/approach behaviors. Recent
500 evidence does indeed suggest that cortical inputs to the LHA participate in the encoding of
501 behavioral transitions, including those linked to feeding[44].
502 Overall, these data suggest that the mPFC-LHA network activity, while not indispensable for
503 regular food intake, does become critically important for excessive intake during stress-driven
504 hyperphagic states. This may be due to pathway activity indicating further energy needs,
505 overriding satiety states and/or by causing continued food engagement to facilitate excessive
506 intake in short periods of time.
507
508 <u>The mPFC-LHA is not a singular pathway, but a multi-branched network</u>

509 Rather than a singular pathway, we now show that the mPFC-LHA network is composed of
510 multiple branches, that can have diverse functions. mPFC neurons innervate multiple LHA
511 subpopulations based on LHA cell type. We observed strong connectivity with LHA_{VGAT} and
512 LHA_{VGLUT2} neurons, and with LHA_{OREX} and LHA_{MCH} neurons, which according to transcriptomic
513 analyses represent glutamatergic VGLUT2-positive subsets[18]. In the current study we also
514 identified that mPFC-innervated glutamatergic LHA neurons project to multiple downstream
515 targets, including VTA, LHA and Peri-PVN. Within the current study we did not further
516 investigate distinct projection targets of mPFC-innervated LHA GABAergic or specific
517 neuropeptidergic populations, but it is likely that these too will have multiple distinct targets[15].
518 Global mPFC-LHA pathway manipulation or measurement studies therefore need to consider
519 that the effects observed represent the net total of multiple sub-pathways, which likely can be
520 in part functionally distinct from each other.
521 To what extent are these branches within the mPFC-LHA network anatomically distinct from
522 each other, as opposed to representing collaterals? At the LHA level prior evidence does suggest
523 that for instance LHA glutamatergic neurons with distinct output targets are at least distinct
524 subsets. Such as LHA_{VGLUT2}-VTA and LHA_{VGLUT2}-LHb neurons, which are anatomically and
525 molecularly distinct sets[28]. At the level of the mPFC, it is an open question to which extent
526 different or the same mPFC neurons innervate distinct LHA neuronal subsets (e.g. LHA_{GABA}
527 versus $LHA_{GLUTAMATE}$). However, our ensemble-based tagging experiments do indicate that there
528 is at least not full collateralization. We observed that there are mPFC neurons that when
529 stimulated do synapse onto glutamatergic but not on GABAergic LHA neurons, or that even
530 synapse on specific neuropeptidergic populations such as LHA_{MCH} neurons.
531 Further studies will need to unravel the exact identity of how distinguishable mPFC neurons are
532 embedded in different anatomical and functional branches within the larger mPFC-LHA
533 network.
534
535 <u>The mPFC projections to LHA and its glutamatergic neurons as a (social) stress integrator</u>
536 In this study we captured single cell dynamics of mPFC cells projecting to the LHA during social
537 stress experiences with *in vivo* electrophysiology. We observed a heterogeneous response of

538 these cells, with some excited and some inhibited. Bulk photometric calcium recordings
539 reflected a biphasic population level response, which on the basis of our in vivo
540 electrophysiology data we consider to be likely mediated by separate subsets of neurons. There
541 was a modest enrichment of stress-modulated responses within the mPFC-LHA pathway
542 compared to non-optotagged mPFC neurons, in accordance with findings that also other mPFC
543 pathways are stress-sensitive[7]. Social stress is a naturalistic but complex stimulus (e.g. featuring
544 stress, social interaction, pain, movement). Social interaction in itself can modulate mPFC-
545 LHA[20,31,42], but it is likely that the stressful aspects of the stimulus are also engaging the
546 network. Our patch clamp data showed also that restraint stress, which has very different
547 features from social stress as an experience (e.g. non-social vs social, immobilization vs bursts of
548 movement), caused increased food intake and similar synaptic alterations at mPFC-LHA_{VGLUT2}
549 synapses as did social stress. Also, a previous studied has shown that the mPFC-LHA pathway is
550 sensitive to another type of aversive stimulus, namely air puff stimuli[21].
551 Our in vivo electrophysiology studies show that during stress some neurons exhibit an increase
552 in activity and others a decrease. Given the multiple type of connections made downstream in
553 the LHA it is possible that these different stress-induced responses in mPFC neurons correspond
554 to distinct branches of the mPFC-LHA network. There is evidence to suggest that at least mPFC
555 neurons projecting to LHA glutamatergic neurons are amongst those that are excited by social
556 stress. Our previous work showed that glutamatergic LHA neurons themselves show an
557 immediate strong excitation during social stress[3], and we here show that a high percentage of
558 these neurons (~80%) receive excitatory input from the mPFC. Furthermore, in the current
559 study we show that activity in these LHA glutamatergic neurons during social stress is
560 indispensable for the subsequent hyperphagia. We also demonstrate that optogenetically
561 stimulating stress-recruited mPFC ensemble projections to glutamatergic LHA subsets can drive
562 feeding. Overall these findings point to mPFC control over LHA glutamatergic neuronal subsets
563 as a key substrate in driving stress-driven feeding.
564
565 <u>Stress-driven plasticity within mPFC-LHA circuits</u>

566 After social stress, at a time point where mice would overeat[3], we observed synaptic changes at
567 mPFC-LHA$_{VGLUT2}$ synapses. On a population-level, patching LHA$_{VGLUT2}$ neurons without knowing
568 their downstream target, we observed evidence for weaker mPFC glutamatergic input on these
569 cells, via reduced release probability selectively at mPFC synapses onto LHA$_{VGLUT2}$ neurons.
570 Interestingly, many LHA$_{VGLUT2}$ cells are linked to a role in curtailing food intake[15,17].
571 Consequently, a reduction of the excitatory input on such neurons could be in accordance with
572 a weakening of a brake on the drive for food intake. A finer grained analysis revealed that the
573 effect of stress on mPFC synapses onto LHA$_{VGLUT2}$ cells was further dependent on the projection
574 targets of the hypothalamic cells. We observed evidence for weakened glutamatergic mPFC
575 synapses onto those LHA$_{VGLUT2}$ cells projecting to a midline hypothalamic region, which indeed
576 upon stimulation curtails food intake[45]. Oppositely, we found that glutamatergic mPFC synapses
577 onto LHA$_{VGLUT2}$ cells projecting to the VTA exhibit potentiation after stress. This latter finding is
578 in accordance with our recent report that after social stress LHA$_{VGLUT2}$ projections to VTA
579 dopamine neurons become potentiated and that this plays a causal role in excess food intake[3].
580 LHA$_{VGLUT2}$ cells have several more projection targets than the ones investigated here[46], which
581 may also be changed by stress. Therefore, the analysis of these specific projections is not meant
582 to be exhaustive, but it illustrates that mPFC synaptic contacts onto distinct LHA$_{VGLUT2}$
583 subpopulation are divergently affected by social stress.
584 Aside from mPFC-LHA branches that did exhibit stress-driven plasticity, there were also several
585 that did not (e.g. mPFC synapses onto LHA$_{VGAT}$ neurons). Of note is that even if mPFC synapses
586 onto LHA$_{VGAT}$ neurons did on average not show stress-driven plasticity, these connections are
587 still engaged when stimulating the mPFC-LHA pathway, potentially contributing to increasing
588 food intake. The findings of plasticity in certain branches, should then also be observed in the
589 context of the network as a whole. We do not claim here that one particular sub-branch is solely
590 responsible for stress-driven feeding. Rather, stress has multiple actions in the network. mPFC-
591 LHA branches (conditionally) linked to promoting food intake are either strengthened or
592 unaffected by the stress experience, whereas branches linked to promoting food intake are
593 either weakened or unaffected. As a whole, this likely gears the mPFC-LHA network more
594 towards favoring further intake of palatable food.

595 One relevant aspect that our study did not address is the extent to which individual animals may
596 be more prone to exhibiting stress-driven overconsumption of palatable food, and whether this
597 depends on individual differences in alterations in the mPFC-LHA pathway. Chronic social stress
598 has known heterogeneous effects between mice on metrics such as willingness to engage in
599 social interactions and extent of induced anhedonia. Classification systems of (distinct types) of
600 stress-susceptible and unsusceptible animals[47,48] have been informative in this regard. Future
601 studies will need to address whether moderate social stress effects on increased palatable food
602 intake, and/or on related eventual weight gain over time[23] also cluster in distinct behavioral
603 profiles.
604
605 Different types of mPFC-LHA stimulation result in different outcomes regarding food intake
606 Prior studies showed that chemogenetic (i.e. likely strong and continuous) or high frequency
607 optogenetic stimulation of the mPFC-LHA pathway reduced intake of chow in mice[21]. Here we
608 show with our global pathway manipulations that optogenetic stimulation of the mPFC-LHA
609 network, at least at lower frequencies can increase food intake. We found that continuous
610 periods of 5 Hz stimulation drove food intake, whereas continuous periods of 1 Hz or 10 Hz
611 stimulation did not. Interestingly, a previous study reported that 5Hz optogenetic stimulation of
612 LHA projections to the VTA could more potently drive food intake than either 2.5Hz or 20Hz[19].
613 The lack of effect on food intake of mPFC-LHA 1 Hz stimulation may have been due to
614 insufficient engagement of the mPFC-LHA network. Continuous 10 Hz stimulation was
615 qualitatively distinct from 5 Hz stimulation in terms of its effect on food intake. This could not
616 be explained by an ineffective stimulation in itself, as animals exhibited more locomotor activity
617 to the 10 Hz stimulation, which in itself might have contributed to the lack of increased intake of
618 food as compared to stimulating the pathway with 5Hz. At the mechanistic level, our *ex vivo*
619 data showed however that over time 10 Hz stimulation of mPFC inputs was less easily followed
620 by LHA_{VGAT} neurons than by LHA_{VGLUT2} neurons in terms of synaptic transmission fidelity. It is
621 therefore possible that the lack of a 10 Hz effect was more due to the continuous nature of
622 delivery rather than the frequency per se. These data together with previous reports, show that
623 distinct ways of mPFC-LHA stimulation can produce differential effects on feeding behaviors,

624 possibly by striking a different balance in the sustained engagement of distinct mPFC-LHA
625 subbranches.
626
627 Overall, our work identifies the mPFC-LHA as a multi-branched network, with an important role
628 in particular for mPFC control over glutamatergic LHA neuronal populations with regards to
629 integrating information about stress and the subsequent excess in the intake of palatable food
630 sources such as fat after stress. These findings may ultimately be relevant in the context of
631 eating disorders in which stress triggers bouts of binge eating behavior.
632

633 **Methods**

634

635 **Animals**

636 In all experiments naïve adult male mice were used (20-35 g, >6 weeks). C57Bl6J (Jax #664),
637 Vglut2-Cre[49] heterozygous (Jax #28863), VGAT-Cre[49] heterozygous (Jax #016962) and TRAP2
638 heterozygous[36] (Jax #030323), animals were bred in-house but originated from the Jackson
639 Laboratory. Swiss-CD1 mice (35-45 g, >12 weeks), were purchased from Janvier (France). All
640 mice (except Swiss-CD1 mice) were group-housed (2-5 per cage) unless otherwise specified.
641 Mice were housed in a 12:12 light/dark cycle (lights on at 07:00 a.m.) at 22 ± 2° C (60-65%
642 humidity). Unless otherwise specified (during brief binge eating recording sessions, see below),
643 animals had access to ad libitum water and lab chow (3.61 kcal/g, CRM (E), 801730, Special
644 Diets Services). Experiments were approved by the local animal welfare body (AWB, or IvD in
645 Dutch) of Utrecht University / University Medical Center Utrecht, and by the national authority
646 (CCD). Experiments were conducted in agreement with the Dutch law (Wet op de Dierproeven,
647 2014) and the European regulations (Guideline 86/609/EEC).

648

649 **Stereotaxic surgery**

650 For stereotactic surgery, all mice were anesthetized with ketamine (75mg/kg i.p.; Narketan,
651 Vetoquinol) and dexmedetomidine (1mg/kg i.p.; dexdomitor, Vetoquinol). Lidocaine (0.1ml;
652 10% in saline; B. Braun) was injected under the skin on the skull a few minutes before surgery.
653 Eye ointment cream (CAF, Ceva Sante Animale B.V.) was applied before surgery. All mice were
654 at least 6 weeks of age at the time of surgery. Animals were fixed on a stereotactic frame (UNO
655 B.V.) and kept on a heat pad during surgery (33° C). When animals were implanted with either
656 optic fibers or cannulas the skull surface was scratched with a scalpel and phosphoric acid (167-
657 CE, ultra-Etch, ultradent, USA) was applied for 5 minutes to roughen the surface at the start of
658 surgery. Injections were done using a 31G metal needle (Coopers Needleworks) attached to a 10
659 µl Hamilton syringe (model 801RN) via flexible tubing (PE10, 0.28 mm ID, 0.61 mm OD, Portex).
660 The Hamilton syringe was controlled by an automated pump (UNO B.V. -model 220). Injections
661 were done bilaterally unless otherwise specified and volumes ranged between 250 and 300 nl

662 per side, at an injection rate of 100 nl/min. The injection needle was retracted 100 µm, 9 min
663 after the infusion and withdrawn completely 10 min after the infusion. The skin was sutured
664 post-surgery (V926H, 6/0, VICRYL, Ethicon). Animals were then subcutaneously injected with the
665 dexmedetomidine antagonist atipamezole (50 mg/kg; Atipam, Dechra), carprofen (5 mg/kg,
666 Carporal) and 1 ml of saline and left to recover on a heat plate of 36° C. Carprofen (0.025 mg/L)
667 was provided in the drinking water for one week post-surgery. Animals were single-housed
668 post-surgery and rejoined with their cage mates three days after surgery, unless otherwise
669 stated.
670
671 *For ex vivo optogenetic-assisted electrophysiology experiments:*
672 For transgenic lines: VGAT-Cre and Vglut2-Cre, mice were injected with AAV5-Syn-CoChR-GFP
673 (3.8*10^12 gc/ml; 300nl; UNC Vector Core) in mPFC (+1.8mm anterior to bregma; 0.90 mm
674 lateral; -2.2 mm ventral from skull under an angle of 10°) and injected with AAV5-hSyn-DIO-
675 mCherry (3*10^12 gc/ml; 300nl; Addgene) in LHA (-1.3 mm posterior to bregma; 1.9 mm lateral;
676 -5.4 mm ventral from skull under an angle of 10°) to visualize GABAergic neurons in VGAT-Cre
677 mice and glutamatergic neurons in Vglut2-Cre mice.
678 To visualize neuropeptide populations in LHA, we used C57bl6 mice, they were injected with the
679 same protocol for the mPFC than the Vglut2-Cre and VGAT-Cre. Mice were injected with rAAV5-
680 MCHpr-Gq-mCherry (1*10^12 gc/ml) for labelling the MCH populations and with AVV5-
681 hORXpr1-3TdTomato (1*10^12 gc/ml) for the Orexinergic neurons. Both were injected in the
682 LHA with the same coordinate and volume than for the transgenic mice.
683 To identified glutamatergic LHA neurons projecting to LHb, VTA and Peri-PVN, we used a Cre-
684 dependent retrograde tracer retroAAV-hSyn-DIO-mCherry (2.8*10^12 gc/ml; Addgene) in
685 Vglut2-Cre mice. Mice were then injected in one of these areas: in the LHb (-1.6 mm posterior to
686 bregma; 1.2 mm lateral; -3.05 mm ventral from skull under an angle of 15°), in VTA (-3.2 mm
687 posterior to bregma; 1.65 mm lateral; -5.0 mm ventral from skull under an angle of 15°) and
688 Peri-PVN (-0.8 mm posterior to bregma; 1.1 mm lateral; -5.4 mm ventral from skull under an
689 angle of 10°). Mice were also injected in mPFC with AAV5-Syn-CoChR-GFP.
690

691

692

693 *For ex vivo TRAP-assisted electrophysiology experiments:*

694 VGAT-cre::TRAP2 and Vglut2-cre::TRAP2 mice were first injected in mPFC with rAAV5-Syn-Flex-
695 CoChR-GFP (4.4*10^12 gc/ml; UNC Vector Core). After a minimum of two weeks, mice went
696 under stress and tamoxifen i.p injection (25mg/kg). After a minimum of one week, mice were
697 injected in LHA with AAV5-hSyn-DIO-eGFP (1*10^12vc/ml; Addgene) and co-injected with
698 rAAV5-ORXpr1-3TdTomato (1*10^12 gc/ml) or rAAV5-MCHpr-Gq-IRES-mCherry (1*10^12
699 gc/ml). To manipulate the mPFC ensemble-LHA, TRAP2 mice were bilaterally also injected with
700 rAAV5-Syn-Flex-CoChR-GFP (4.4*10^12 gc/ml; UNC Vector Core, mPFC: +1.8mm anterior to
701 bregma; 0.90 mm lateral; -2.2 mm ventral from skull under an angle of 10°) and optic fibers
702 (diameter 200 µm; FT200UMT, 0.39NA, Thorlabs, Germany) fitted with ceramic ferrules (230µm
703 bore size, Precision Fiber Products, MM-FER2002, USA or Thorlabs, CFLC230-10, Germany) were
704 implanted bilaterally in the LHA (-1.2 mm posterior to bregma; 1.85 mm lateral; -4.85 mm
705 ventral from skull under an angle of 10°). After surgery mice were housed collectively for at
706 least 6 weeks.

707

708

709 *For in vivo optogenetic experiments:*

710 To drive the mPFC-LHA pathway at various frequencies, C57BL6 mice >3 months of age were
711 bilaterally injected with the light-sensitive Channelrhodopsin variant CoChR (300 nl rAAV5-Syn-
712 CoChR-GFP at a titer of 3.8*10^12 gc/ml) or a fluorophore for control animals (300 nl rAAV5-
713 Syn-eYFP, titer of 5.6*10^12 gc/ml) (Penn Vector Core, USA) in the mPFC (AP +1.8; ML ±0.92
714 mm from bregma; DV -2.24 mm from the skull at a 10° angle; 100 nl/min). After injection a 10-
715 min delay was implemented and, two minutes before retraction, the needles were lifted 100
716 micrometers to allow for proper diffusion of the virus. To stimulate mPFC axon terminals
717 innervating the LHA, optic fibers (diameter 200 µm; FT200UMT, 0.39NA, Thorlabs, Germany)
718 fitted with ceramic ferrules (230µm bore size, Precision Fiber Products, MM-FER2002, USA or
719 Thorlabs, CFLC230-10, Germany) were targeted to the lateral hypothalamus and implanted

720 bilaterally at AP -1.2; ML ±1.85 from bregma and DV -4.85 mm from the skull under a 10° angle.
721 The implants were fixed to the skull using 2 stainless steel screws, C&B-Metabond (Parkell Inc.,
722 USA), and dental cement (GC Corporation, Japan). After surgery mice were individually housed
723 for the remainder of the experiment.
724 For the optogenetic stimulation of the LHA_{VGLUT2}-periPVN pathway, the optogenetic procedure
725 of surgery remained the same, vglut2-cre mice were injected bilaterally with the light-sensitive
726 Channelrhodopsin variant CoChR (300 nl rAAV5-Syn-Flex-CoChR-GFP 2.2*10^12 gc/ml, UNC
727 Vector Core) or with the fluorophore for control (300 nl rAAV5-Syn-DIO-GFP 2.2*10^12 gc/ml,
728 Addgene) in LHA (-1.2 mm posterior to bregma; 1.85 mm lateral; -4.85 mm ventral from skull
729 under an angle of 10°), and the optic fibers were place above the peri-PVN (-0.8 mm posterior to
730 bregma; 1.1 mm lateral; -4.85 mm ventral from skull under an angle of 10°).
731 After surgery Vglut2-cre mice were housed collectively for at least 8 weeks for the PFC-LHA_{VGLUT2}
732 experiments and a minimum of 6 weeks for LHA_{VGLUT2}-periPVN.
733
734
735 *For in vivo chemogenetic experiments*
736 The pAAV-hSyn-DIO-hM4D(Gi)-mCherry (DREADD virus) (4*10^12 gc/ml, Addgene, United
737 States, addgene.org) or pAAV-hSyn-DIO-mCherry (4.2*10^12 gc/ml, Addgene, United States,
738 addgene.org) were bilaterally injected into the mPFC, (in mm: +1.8AP, -1.2ML from Bregma and,
739 -2.3 DV, from skull, at a 10° angle) with an injection-rate of 100 nl/min, and a volume of 300 nl.
740 The Cav2-cre-virus (2*10^12 gc/ml, Plateforme de Vectorologie de Montpellier, https://plateau-
741 igmm.pvm.cnrs.fr/), combined with red-retrobeads (60x dilution, Lumafluor Inc, lumafluor.com)
742 for injection site verification, was bilaterally injected into the anterior LHA (in mm: -1AP,
743 1.85ML, 5.36DV from Bregma, at a 10° angle), and posterior LHA (in mm: -1.85AP, 1.9ML,
744 5.41DV, from Bregma, at a 10° angle) with an injection-rate of 100nl/min. After injection of the
745 viral construct, the needle was kept in place for 8 minutes after which it was retracted for 100
746 um and left in place for two more minutes to allow proper diffusion of the virus. Thereafter, the
747 needle was fully subtracted at a slow pace. After injection, the skin was sutured (V926H, 6/0,

748 VICRYL, Ethicon). After surgery mice were individually housed for the remainder of the
749 experiment.
750 For experiments where we optogenetically stimulated mPFC-LHA while having chemogenetic
751 control over LHA_{VGLUT2} neurons we used VGLUT2-cre mice. The pAAV-hSyn-DIO-hM4D(Gi)-
752 mCherry DREADD virus (300 nl 4*10^12 gc/ml, Addgene, United States) was injected in the LHA
753 and to combined with the optogenetic optic fibers were implanted bilaterally in the LHA (-1.2
754 mm posterior to bregma; 1.85 mm lateral; -4.85 mm ventral from skull under an angle of 10°)
755 and the light-sensitive Channelrhodopsin variant CoChR (300 nl rAAV5-Syn-CoChR-GFP at a titer
756 of 3.8*10^12 gc/ml, UNC Vector Core) was injected bilaterally in the mPFC (+1.8mm anterior to
757 bregma; 0.90 mm lateral; -2.2 mm ventral from skull under an angle of 10°).
758
759 *For in vivo electrophysiology with optrode experiments*
760 To identify mPFC neurons that project to the LHA in electrophysiological recordings we used a
761 dual viral approach. First the Cav2-cre-virus (2*10^12 gc/ml, Plateforme de Vectorologie de
762 Montpellier, https://plateau-igmm.pvm.cnrs.fr/) was injected, combined with red-retrobeads
763 (60x dilution, Lumafluor Inc, lumafluor.com) for injection site verification, into LHA (in mm: -
764 1.3AP, 0.9 ML, -5.3DV from Bregma, 0° angle). A second virus pAAV-EF1α-doublefloxed-
765 hCHR2(H134R)-mCherry was injected at two locations in the mPFC (+1.8 mm AP, -0.45 mm ML, -
766 2.5 mm DV and +1.8 mm AP, -0.45 mm ML, -1.8 mm DV from Bregma, 0° angle, 100-150nl per
767 site and a titer of 2-4*10^12 gc/ml). All injections were done unilateral and targeting the left
768 hemisphere, except for 2 mice which received a bilateral injection in the LHA. Injections for
769 electrophysiological recordings were done using glass pipettes (#504949, World precision
770 instruments) coupled to a Nanojet injector (#504127, World Precision Instruments). To allow for
771 proper expression of the virus before electrophysiological recordings, the optrode was placed in
772 a second surgery, >3 weeks after viral injections, in the left mPFC (+1.8mm AP, -0.5mm ML from
773 Bregma, -2.0mm DV from the surface of the brain). During this surgery a craniotomy was made
774 above the mPFC and the dura removed, whereafter the optrode was inserted in the brain using
775 a micromanipulator (Scientifica, UK). Two screws were placed in the skull for attachment of the
776 optrode to the skull and the ground was placed through a small hole in the skull on the

777 cerebellum and fixed with a small drop of superglue. After closure of the craniotomy with
778 silicone, the whole implant was fixed with C&B-Metabond (Parkell Inc., USA), and dental cement
779 (GC Corporation, Japan). Recordings during behavior were made at least 3 weeks after
780 implantation of the optrode to allow for proper recovery. After surgery mice were individually
781 housed for the remainder of the experiment.
782
783 *For in vivo fiber photometry experiments:*
784 For *in vivo* fiber photometry we unilaterally injected a retrograde CAV2-cre virus (2x10^12
785 gc/ml, 200 nl per site) in the LHA (AP -1.0; ML 1.85; DV -5.40 & AP -1.85; ML 1.9; DV -5.40) and
786 rAAV-syn-FLEX-jGCaMP8s-WPRE (3*10^12 gc/m, 300 nl) in the PFC (AP+1.8; ML 0.90; DV -2.2) of
787 C57BL/6 mice. Next, we inserted an optical fiber (ø400 µm, Thorlabs) above the injection site
788 (DV: -1.9). We fixated the fiber with superbond glue (Sun Medical Co.), and dental cement (Fuji
789 PLUS-capsules, G.C. corporation). After the surgery, mice were allowed to recover for 4 weeks,
790 while being socially housed, before the behavioral recordings started to ensure virus expression.
791
792 **Patch-clamp Electrophysiology**
793 After a minimum of six weeks following surgery, mice were anesthetized with isoflurane (Zoetis,
794 UK) in the morning and were then rapidly decapitated. Coronal brain slices of 250 µm were cut
795 on a vibratome (1200 VTs, Leica, Rijswijk, The Netherlands) in ice-cold carbogenated (95% O2,
796 5% CO2) cutting solution, which contained (in mM) choline chloride (92); ascorbic acid (10);
797 CaCl2 (0.5); glucose (25); HEPES (20); KCl (2.5); N-Acetyl L Cysteine (3.1); NaHCO3 (25);
798 NaH2PO4 (1.2); NMDG (29); MgCl2 (7); sodium pyruvate (3); Thiourea (2). Slices were
799 transferred for 5-10 min to a warmed solution (34 °C) of the same composition, before they
800 were kept at room temperature in carbogenated incubation medium, which contained (in mM):
801 ascorbic acid (3); CaCl2 (2); glucose (25); HEPES (20); KCl (2.5); NaCl (92); NaHCO3 (20);
802 NaH2PO4 (1.2); NMDG (29); MgCl2 (2); sodium pyruvate (3) and Thiourea (2). During recordings,
803 slices were immersed in artificial cerebrospinal fluid (ACSF) containing (in mM): NaCl (124); KCl
804 (2.5), CaCl2 (2.5); glucose (11); HEPES (5); NaHCO3 (26); NaH2PO4 (1); MgCl2 (1.3) and were
805 continuously superfused at a flow rate of 2 ml min−1 at 32° C.

806

807 Neurons were patch-clamped using borosilicate glass pipettes (2.7–4 MΩ; glass capillaries,
808 GC150-10, Harvard apparatus, UK), under a BX51WI Olympus microscope (Olympus, France).
809 For voltage or current clamp recordings, signal was amplified, low-pass filtered at 2.9 kHz with a
810 4-pole Bessel filter and digitized at 20 kHz with an EPC9/2 dual patch-clamp amplifier (HEKA
811 Elektronik GmbH). Data were acquired using PatchMaster v2x78.2 software. After break-in, 10
812 minutes of waiting time occurred prior to the start of the recording. Series resistance was
813 determined in Voltage clamp with a −4 mV step from -65 mV to -69 mV lasting 50 ms, using the
814 resultant capacitive current transients and Ohm's law. Light pulses (470 nm, 1 ms; 25.4mW)
815 were delivered with a pE-4000, CoolLed, UK illumination system. All electrophysiological
816 measures are recorded with a 10 seconds inter sweep interval (0.1Hz) and all data points are
817 shown as an average of 10-20 sweeps, unless otherwise specified.

818

819 *Paired-pulse ratio (PPR):* PPR experiments were performed with cesium methanesulfonate-
820 based internal medium, containing (in mM) cesium methanesulfonate (139), CsCl (5), HEPES
821 (10), EGTA (0.2), creatine phosphate (10); Na2ATP (4); Na3GTP (0.3); MgCl2 (2). Averaged
822 AMPAR-mediated currents in LHA neurons were measured in response to optogenetic
823 stimulation of mPFC terminals using two pulses with a 60, 100 or 200 ms inter-pulse interval and
824 measuring the resulting peak amplitude of the two synaptic responses. The PPR was calculated
825 by dividing the amplitude of the synaptic response to the 2nd pulse by the amplitude of the
826 synaptic response to the 1st pulse.

827

828 *NMDAR-AMPAR ratios:* Synaptic LHA optogenetically evoked AMPAR and NMDAR currents were
829 measured in response to a single light pulse. Recordings were made in voltage clamp with the
830 aforementioned cesium methanesulfonate-based internal medium. Under these conditions, it
831 was possible to detect inward glutamatergic currents (at −65 mV) and NMDAR (at 40mV at 100
832 ms). Experiments were done in the presence of 100 µM picrotoxin, to block potential $GABA_A$
833 receptor contributions. The NMDA/AMPA ratio was calculating by dividing the amplitude of the
834 EPSC after 100ms at +40mV by the amplitude of the synaptic response at -65mV.

835

836 *mPFC-LHA connectivity experiments*: Recordings were made in voltage clamp in a cesium
837 methane sulfonate based internal medium as described above. Under these conditions, it was
838 possible to detect inward glutamatergic currents (at −65 mV). Cell type specific connectivity was
839 determined based on whether a neuron showed an optogenetically-evoked synaptic response
840 larger than 5 pA. For monosynaptic confirmation, cells were recorded and opto-stimulated
841 (1ms) once per sweeps, first during at least 15 sweeps with ACSF, then 1µM of TTX was added
842 to ACSF for a minimum of 25 sweeps to observe the effect on the synaptic response and finally
843 100µM 4-AP was added to the mix and recorded for a least 20 sweeps.

844

845 *Intrinsic excitability and mPFC-driven LHA cell firing experiments:* Recordings were made in
846 current clamp in a potassium gluconate based internal containing (in mM), Potassium Gluconate
847 (139); HEPES (10); EGTA (0.2); creatine phosphate (10); KCl (5); Na2ATP (4); Na3GTP (0.3); MgCl2
848 (2). Only LHA cells showing a synaptic response larger than 5pA at -65mV after 1ms of opto-
849 stimulation went under this following protocol. To determine current-voltage relationships and
850 biophysical properties, membrane resistance and firing pattern, cells were recorded in current
851 clamp. Cells were clamped at 0 pA and from there were subjected to 17 subsequent sweeps.
852 Every sweep started with a 0 pA injection of 400 ms, followed by a current step of 800 ms length
853 of -150 pA (with a +25 pA increasing increment on each subsequent sweep), followed by a
854 return to 0 pA for 1000 ms. Inter-sweep interval was 10 seconds.
855 To assess if the opto-stimulation of mPFC inputs was sufficient to fire the LHA neurons, cells
856 were clamped at -50pA to prevent the spontaneous firing and 25 pulses of 1ms were applied at
857 5Hz for 10 sweeps.

858

859 *Spike fidelity over 10 minutes*
860 Recordings were made in current clamp in a potassium gluconate based internal (see above),
861 cells were clamped at 0pA, except if they were spontaneously firing (-20pA or -30pA); and were
862 opto-stimulated during 10 minutes at 1Hz, 5hz and 10hz in a random order. EPSP was counted if
863 the change of amplitude was equal or more than 2mV compared to the overall baseline.

Drugs for patch-clamp experiments

All drugs were obtained from Sigma (UK), Abcam (UK) and Tocris (UK). With the exception of picrotoxin (DMSO, 0.01% final bath concentration) all drugs were dissolved in purified water. Drugs were aliquoted at a concentration of 1/1000th of the final bath concentration and stored at -20°C. Upon use they were thawed and quickly dissolved in the recording medium.

In vivo **electrophysiology recordings**

Recording single unit activity of prefrontal cortical neurons.

Extracellular single-unit activity was recorded using custom-built optrodes. An electrode bundle consisting of 32 individually isolated nichrome wires (12 µm diameter; 80% nickel, 20% chromium; Kanthal, Sandvik Material Technology, Germany) was glued to an optic fiber (Thorlabs, Germany, 200 µm diameter, 0.39NA, with the tip placed at 300-700 µm above the electrodes) to allow for optogenetic identification of mPFC-LHA cells. Electrodes were attached with gold pins to a 32-pin Omnetics connector using an electrode interface board (Open Ephys, www.openephys.org) which was mounted on a 3D printed holder (based on the Flexdrive[50], Open Ephys). The microwires were cut at an angle so that they were organized in a vertical space of 200-400 µm, whereafter they were gold-plated (Neuralynx, United States) to an impedance of 100kΩ using a NanoZ impedance tester (Plexon, United States). The connector was grounded through a bare platinum-iridium wire (127 µm diameter; 90% platinum, 10% iridium; Science Products, Germany) placed on the cerebellum. Analog signals were acquired using a 32-channel RHD2132 headstage (Intan Technologies, USA), bandpass filtered between 2.5 and 7603.88Hz, and digitized at 30 kHz. Data were transferred to the Open Ephys acquisition board using an Intan Technologies Serial Peripheral Interface cable (2.9 mm, interference of the cable during behavior was reduced by counterbalancing the weight of the cable with flexibly moving counterweights) and acquired by the Open Ephys GUI interface (version 0.5.2.2; https://open-ephys.org/gui)[51]. Behavior of the mice was recorded from above the cage using a

893 Blackfly S USB camera (BFS-U3-31S4M-C, Teledyne FLIR) which was synchronized with the
894 electrophysiological data by sending a TTL pulse for every acquired frame (sample rate 30Hz) to
895 the Open Ehpys I/O board. The mice were also recorded front view using a webcam (HD C270,
896 Logitech, Switzerland). This data was synchronised by a light signal generated at a fixed interval
897 by an Arduino controlled LED which light signal was duplicated as a TTL output to the I/O board.
898
899 *Spike sorting.*
900 Before spike-sorting first a common average reference https://github.com/cortex-
901 lab/spikes/blob/master/preprocessing/applyCARtoDat.m[52] was applied to remove common noise
902 contamination across channels. Spikes were then automatically detected and assigned to
903 clusters using the template-matching algorithm of kilosort (version 2.0;
904 https://github.com/MouseLand/Kilosort/releases/tag/v2.0) with the following settings: Ops.Th
905 [10 4], Ops.AUCsplit [0.9], ops.Lam [10], ops.minFR [0.1]. Clustering results were manually
906 checked for waveform shape, stable amplitude over time and the presence of a clear refractory
907 period. Moreover, resembling clusters were assessed to see if nearby clusters belonged to the
908 same cell and were merged when appropriate. Data checking and curation was done in Phy
909 (https://github.com/cortex-lab/phy). After curations in Phy the isolation distance was calculated
910 as a final quality control. Single units with an isolation distance of >20 were included in the
911 dataset [53,54] (Average isolation distance of optotagged mPFC-LHA cells=38.9, Minimum=20.3,
912 Maximum=115.2).
913
914 *Optogenetic identification of mPFC-LHA neurons.*
915 After every behavioral session, we applied short light pulses (2ms) from a 473 nm DPSS laser
916 (CNI Laser, China) with a random 6-9 s interval for ~30 min (over 200 trials) triggered using a
917 microcontroller (Arduino, Italy)) and ~5-8 mW output at the fiber tip above the recording site.
918 Depending on the presence of a voltage-volley during laser stimulation, a window of 1 or 2 ms
919 after the laser onset was blanked. Significant light-induced activation was determined with the
920 stimulus-associated spike latency test (SALT, $p<0.01$; http://kepecslab.cshl.edu/salt.m)[53]. In
921 brief, SALT compares the distribution of first spike latencies relative to the light pulse to epochs

922 of the same duration in the stimulus-free baseline period. Additional criteria were included to
923 prevent inclusion of false-positive neurons through network-related activity: a peak z-
924 score>1.65, average first spike latency < 7ms, jitter < 3.5ms, reliability > 0.03, Pearson's
925 correlation between the average waveform of a cluster and the average waveform of the first,
926 putatively light-evoked spikes > 0.8 and a waveform duration above 550 microseconds (through-
927 to-peak). Similar criteria have been used for mPFC-LHA opto-tagging and ex-vivo data of mPFC-
928 LHA neurons suggest that a first spike latency below 8ms limits false-positive identification of
929 non-expressing neurons through recurrent connectivity [20] and the same criteria were also used
930 in other mPFC opto-tagging studies[53,55,56]. According to these criteria mPFC-LHA neurons could
931 be photo-identified in 12 out of 16 mice that had correct placement of the optrode and proper
932 expression of channelrhodopsin. All broad-spiking neurons that were not positively identified
933 were categorised as non-identified mPFC neurons. To enhance the quality of comparison
934 between opto-tagged and non-identified neurons, we only used non-identified neurons for
935 analysis if in the same mice opto-tagged neurons were present.
936
937
938 ***In vivo* fiber photometry recordings**
939 We used a 2-site photometry system (Doric lenses) to detect calcium and non-calcium
940 dependent dynamics (GFP and isobestic channel). Two light-emitting diode delivered blue (465
941 nm, 40 ± 1 µw in the brain) and purple (405 nm, 20 ± 1 µw in the brain) light, which was guided
942 to the mouse via a mini cube (iIFMC5-G2_IE(400-410)_E(460-490)_F(500-540)_O(580-680)_S)
943 and optical patch cord (ø400 µm). Emitted light was detected with the mini-cube integrated
944 photodetectors and transmitted to the console with different reference frequencies (GFP 572
945 Hz, ISO 209 Hz). The photometry system was controlled by Doric Studio software (version
946 6.3.2.0), which recorded 243 samples per second (50 times decimated). The relative changes in
947 light (ΔF/F) were calculated with custom-made Python scripts (version 3.13.5). Code accessible
948 here: https://doi.org/10.5281/zenodo.18670225.

949 First, outliers were removed (>4 std aways from a mean signal of 9 minutes) and data was
950 smoothed (per 100 data points). We calculated the ΔF/F for each trial with -10 to -2 seconds
951 before the onset as a baseline. Next, the session average and peak signals were extracted.

952

953 **Behavioral paradigms**

954 All behavioral manipulations and tests were performed during the light phase.

955

956 *Two-day Social stress paradigm*

957 The social subordination stress protocol used was designed according to a resident intruder
958 paradigm. The resident, a Swiss-CD1 male previously used for breeding, was housed in a large
959 Makrolon cage (type IV, Tecniplast, Italy), an intruder; an experimental male mouse, was placed
960 in this cage. Fighting time was tracked live and animals were allowed to fight for 20 s, twice a
961 day for two days, one fighting session in the morning (8.30 – 11.00a.m.) and one in the
962 afternoon (16.00 – 18.30p.m.). For the remainder of the day, animals were separated by a
963 perforated transparent splitter, allowing sensory, but no physical interaction. The control
964 animals were co-housed with a non-familiar C57B6J male mouse for two days, preventing
965 physical interaction. This short stress paradigm has been shown to not change body weight in
966 the first days after the stressful experience when food intake is measured[3]. Consistent with this,
967 no difference in body weight were observed between the experimental groups in this study. The
968 schematics on social stress (Fig. 2D and Suppl. Fig. 2C) were created in BioRender. Meye, F.
969 (2026) https://BioRender.com/mula9s9.

970

971 *Limited access choice diet*

972 In the limited access choice diet paradigm, animals were exposed to fat (i.e. tallow; Blanc de
973 Boeuf, Vandermoortele, 9.0 kcal/g) and regular chow for 2 hours a day in a clean cage
974 (Makrolon cage type IV, Tecniplast, Italy). Animals were habituated to the limited access cage
975 and fat, during 3 occasions at least, before the start of the experiment. Animals were subjected
976 to stress as described above and on the day after, fat intake was measured over a 2-hour fat
977 access period, starting between 9 a.m. and 11 a.m.. Unlimited chow was provided the remaining

978 22 h of the day. The figure 1 panel C schematic of the food choice paradigm was created in
979 BioRender. Meye, F. (2026) https://BioRender.com/ayjpdtm.
980
981
982 *Real-time place preference / aversion test*
983 The conditioned place preference test consisted of two sessions separated over two days. The
984 test cage (73x25 cm) consisted of two chambers (30x25 cm) clearly separated by a narrower
985 middle area. The two chambers had different flooring (fine grid vs coarse grid) and different
986 walls (striped vs black) to provide contextual discriminability. In the baseline session mice were
987 allowed to freely explore the test cage. During the test session (20 minutes total duration) one
988 of the compartments (counterbalanced design) was paired with optogenetic stimulation using
989 closed-loop optogenetics. After 10 minutes the stimulation site was paired with the other
990 compartment, to limit effects of a priori preference for one of the compartments. Mice were
991 recorded by a webcam (HD C270, Logitech, Switzerland). Closed-loop optogenetics was
992 established by automatically tracking mice in Bonsai (Open Ephys) which triggered the Master-8
993 pulse generator through an Arduino upon entering the stimulation chamber, in turn triggering
994 the laser at the dedicated frequency as long as the mouse was present in the stimulation
995 compartment. The position of the animal was tracked in the cage offline using Ethovision 9
996 (Noldus, Wageningen). Preference score was calculated by scoring the total time spent in the
997 stimulation compartment divided by the total time spent in the stimulation and non-stimulated
998 compartment. Cages were cleaned in between animals with 70% ethanol.
999
1000 *Food intake video analysis*
1001 Videos were taken from the side of the feeding cage with webcams (HD C270, Logitech,
1002 Switzerland) and acquired using the Windows Camera App or Bonsai. Feeding bout analysis was
1003 done manually and blind for the virus type. Data were acquired over different batches which
1004 were analyzed by an independent observer.
1005
1006 *Recordings during social stress.*

1007 For social stress recordings mice were handled extensively to get used to fixation and getting
1008 used to being attached to the recording cable. During the day of social stress recordings mice
1009 were put into an unfamiliar cage of a CD1 aggressor mouse, which was temporarily removed
1010 from its home cage. After 15 minutes the CD1 mouse was introduced into the cage but physical
1011 contact was prohibited by a transparent barrier. After another 45 minutes the barrier was re
1012 moved and the mice were allowed to physically interact (fight) for a cumulative 20 seconds
1013 whereafter the barrier was put back. This period lasted on average more than 4 minutes. Hence,
1014 during the total stress exposure time physical contact which could introduce noise in the
1015 recording was limited.
1016
1017 *Restraint stress*
1018 This stressor was induced by restraining mice twice a day during 15 minutes each and during
1019 two days. The mice were place individually in a conical Falcon tube (50mL) previously drilled
1020 with thirty holes. Control mice were handled and place back to their home cage after couple
1021 minutes.
1022
1023 *Locomotor activity and time spent in food zones.*
1024 Mice position and speed in the food cage were automatically tracked in real-time from camera
1025 images or offline from the acquired webcam videos using Ethovision (version 9.1; Noldus
1026 Technologies, The Netherlands). Food zones were 9x11 cm in size. Time in the food zone was
1027 determined by calculating the cumulative time spent in the food zone per block of 10 minutes.
1028 The effect of 5Hz stimulation on time in food zone was determined by calculating the difference
1029 in time spent in the food zone during the individual three ON-Blocks with the preceding OFF-
1030 block and consequently taking the average of these three values obtained for the separate ON-
1031 Blocks.
1032
1033 ***In vivo* circuit approaches during behavioral experiments**
1034
1035 *In vivo optogenetic stimulation experiments*

1036

1037 *Optogenetic stimulation of mPFC-LHA in stress-naïve mice:* Before every experiment, mice were
1038 extensively handled and habituated to the food-context, fat and optogenetic cables for at least
1039 2 weeks before the start of the experiment. Mice had an incubation time of at least 12 weeks
1040 after viral injection for this experiment. A single experiment consisted of three baseline days, an
1041 optogenetic stimulation day followed by another non-stimulation day. Mice were also attached
1042 to patch cables on days where no stimulation was applied. Raw food intake was measured on all
1043 days after one hour in which the mice were able to freely feed on regular chow (3.61 kcal/g,
1044 CRM (E), 801730, Special Diets Services) or Tallow (Blanc de Boeuf, Vandemoortele, 9,0 kcal/g).
1045 On stimulation days mice were recorded with a webcam from the top, to allow for later offline
1046 tracking of the position of the mice in the food cages using Ethovision (Noldus, Netherlands). In
1047 a subset of the experiments feeding behavior was recorded from the side using webcams (HD
1048 C270, Logitech, Switzerland). Time of testing across days was kept constant as much as possible.
1049 Different frequencies were tested on the same mice and in the order 5Hz, 10Hz and 1Hz with
1050 one week without stimulation in between each stimulation experiment.

1051

1052 On stimulation days, mice were connected to optogenetic patch cables (Thorlabs, 200 µm, 0.39
1053 NA, FT200UMT) which ended in a ceramic ferrule (230 µm bore size, Thorlabs or Precision Fiber
1054 Products) and connected to the implant through a sleeve (Precision Fiber Products). Cables
1055 were connected to the laser (473 nm DPSS laser, CNI Laser, China) using an FC-connector
1056 (Thorlabs) and via a rotary joint (Doric lenses, Canada), which divided light intensity equally over
1057 the two hemispheres. Light intensity was set to 5mW at the tip of the fiber above the LHA. Light
1058 pulses (5ms duration) at indicated frequencies were applied during blocks of ten minutes using
1059 a Master-8 pulse stimulator (A.M.P.I., Jerusalem, Israel) and were alternated with non-
1060 stimulation blocks of similar length. Mice were single-housed and food and water were present
1061 ad libitum in the home cage.

1062

1063 *Optogenetic stimulation of mPFC-LHA in control versus stressed mice:*

1064 Viral incubation time and experimental setup for optogenetic stimulation is similar as described
1065 above. 5Hz stimulation was applied in alternating OFF and ON blocks with a duration of ten
1066 minutes. Mock-stimulated animals were attached to patch-cables and laser-stimulated, but light
1067 transmission was completely blocked in the connecting sleeve on the head of the animal. For
1068 this experiment in particular, mice were habituated to fat (three times) in the food context and
1069 to optogenetic cables in the test cage for two weeks. Baseline food intake was measured 4-5
1070 days before exposure to stress. During this session animals were similarly attached to patch
1071 cables but no stimulation was applied. Social stress paradigm was performed as described[3].
1072 C57BL6 mice were introduced into a cage (Makrolon cage, type IV, Tecniplast, Italy) of an
1073 aggressor mouse (CD1, Janvier) and subjected to 4x 20s of physical fight over the course of two
1074 days (one fight in the morning and one in the afternoon) after which they were separated by a
1075 transparent wall for the remainder of the time. The cage of the Swiss-CD1 male mice contained
1076 enrichment that was previously used in the home cage, while the cage part of the experimental
1077 C57BL6 mice was enriched with 3 tissues. Food and water were present ad libitum as in the
1078 stress and home cage. Control mice were subjected to 2 days of cohousing with a conspecific in
1079 the same cage, but separated by a transparent wall. On the day after stress mice were put
1080 directly from the stress-context into the food context and returned to their home cage
1081 afterwards. One mouse was excluded from analysis on the basis of being a large statistical
1082 outlier. Three mice were excluded due to technical problems (e.g. malfunctioning video
1083 recording). All mice were individually housed during the experiment and had ad libitum access
1084 to food and water.
1085
1086 *Optogenetic stimulation of mPFC$_{SOCIAL\ STRESS}$ ensemble projections to LHA:*
1087 Mice were extensively handled and received mock intraperitoneal injections couple days before
1088 to be expose to an acute social stress (20scs) and received tamoxifen i.p injection (25mg/kg)
1089 three hours later. Control mice were placed in new cage with another C57Bl6 mice separated by
1090 a perforated wall and received tamoxifen 3 hours later as well. After a minimum of 6 weeks,
1091 mice were handled and habituated to the food-context, fat and optogenetic cables. After at
1092 least two baseline days in the 2-choice paradigm, mice were tested in this paradigm during one

1093 hour, during which there was 5 Hz stimulation, presented in a pattern of 3 seconds on (5 Hz
1094 stimulation), 1 second off.
1095
1096 *Optogenetic stimulation of* the *LHA_{VGLUT2}-periPVN pathway experiment in stress-naïve mice.*
1097 The experimental setup is similar to the $mPFC_{SOCIAL\ STRESS}$ ensemble-LHA pathway experiment,
1098 but the mice were only stimulated at 10Hz (alternation of 3 seconds ON, 1 second OFF).
1099
1100 *In vivo chemogenetic inhibition experiments*
1101
1102 *Chemogenetic inhibition of mPFC-LHA pathway in control versus stressed mice during food*
1103 *intake.*
1104 Mice were extensively handled and habituated to the food context (3 times) and fixation and
1105 mock intraperitoneal injections for at least two weeks. First, mice were tested for their baseline
1106 fat and chow intake in the 2-choice context (2 hours). For this baseline test, they received an
1107 intraperitoneal saline injection (150 µl) to rule-out a potential effect of stress of this procedure.
1108 Baseline measurements were done at least 4 days before being subjected to stress to prevent
1109 any influence of palatable food intake on their susceptibility to stress. The 2day social stress
1110 paradigm was done as described above. CNO was made fresh on the day of testing and applied
1111 at a dose of 5 mg/kg, 45 minutes before being placed in the food context. Mice removed from
1112 the stress context were injected with CNO and placed back in their home cage with ad libitum
1113 food before being put in the food context. Similarly, for the acute stress experiment mice
1114 received the CNO injection 45 minutes before being place in the food context and 25 minutes
1115 prior to stress. All mice were individually housed during the experiment and had ad libitum
1116 access to food and water. Two mice were excluded due to technical problems.
1117
1118 *Chemogenetic inhibition of* LHA_{VGLUT2} neurons during *optogenetic stimulation of mPFC-LHA.*
1119 Mice were extensively handled and habituated to the food-context, fat and optogenetic cables
1120 and mock intraperitoneal injections for at least 2 weeks before the start of the experiment.
1121 Experimental setup is similar as described above, as well as the dose of CNO (5 mg/kg) 45

1122 minutes before being place in the food context, expect that the mice were not exposed to stress
1123 and will be optogenetically stimulated at 5Hz (alternation ON/OFF every 10 minutes). To ensure
1124 that the food intake measured during this experiment is not due to ceiling effect, on the last day
1125 mice were deprived of food for 21h and re-expose two hours to the 2-choice context.
1126
1127 *Chemogenetic inhibition of* LHA_{VGLUT2} neurons during stress.
1128 Mice were habituated to the food context several days prior to the experiment. Mice then
1129 either experienced (40 seconds; ~5 minutes), on each of two consecutive days, social stress via a
1130 CD1 aggressor, or instead a control experience by co-housing with a novel conspecific. On both
1131 days, 45 minutes prior to the experience, the mice received an i.p. injection of 5mg/kg CNO.
1132 Food intake was monitored the subsequent day during 2 hours.
1133
1134 *In vivo fiber photometric recordings during stress and feeding.*
1135 Mice were exposed to lard and chow in an operant chamber (ENV-008CT) for 90-minute
1136 sessions. Food contacts were detected via infrared beam breaks (ENV-254-FB) and recorded
1137 using MED Associates software (MED-IV). From these recordings, we extracted total eating
1138 duration and the number of eating bouts. An eating bout was defined as a continuous period of
1139 food contact lasting at least one second, with successive contacts separated by less than one
1140 second considered part of the same bout. Once the mice were habituated to the eating
1141 procedure, we recorded their neural activity photometrically during eating under baseline
1142 conditions. For the post-stress eating recordings, we employed a crossover design in which the
1143 order of conditions was pseudo-randomly determined using RandoMice[57], accounting for signal
1144 strength, fiber efficiency, and initial recording time. During this protocol, mice were subjected to
1145 the two-day social defeat paradigm as described previously. On the day following the defeat
1146 sessions, photometric recordings were performed again while the mice were eating. A recovery
1147 period of two weeks was provided between stress and control sessions. To record mPFC–LHA
1148 activity during social stress, we first conducted a three-minute baseline recording in the
1149 subject's home cage to minimize stress and allow for photobleaching. The subject was then
1150 exposed to a CD1 aggressor mouse in the aggressor's home cage while simultaneous

1151 photometric and video recordings were obtained. The mice were allowed to engage in fighting,
1152 and recordings were terminated after 40 seconds of active fighting. Video recordings were used
1153 to manually score for aggressive behaviors, including slamming, biting, chasing, and aggressive
1154 standing, but not approach behaviors, with one-second temporal precision. The offset of each
1155 fight was defined as the end of the interaction or, when applicable, the landing of the C57BL/6
1156 mouse. Aggressive behaviors occurring less than one second apart were considered part of a
1157 single fighting bout.
1158
1159
1160 **Histology and microscopy**
1161 For each recording the virus injection sites, as well as the placement of optic fibers and/or the
1162 optrodes were examined. Only data obtained from mice with correct placements were included.
1163 After experiments, mice were anesthetized with pentobarbital (75-100 mg/kg) and
1164 transcardially perfused with Phosphate-Buffered Saline (PBS) containing 4% paraformaldehyde
1165 (PFA). Brains were post-fixed in 4% PFA overnight and transferred to PBS. Before slicing, brains
1166 were embedded in 4% agarose to maintain structural integrity. Coronal sections of the entire
1167 brain were sliced at 60um using a vibratome (VT1000s, Leica, Rijswijk, The Netherlands). For
1168 patch clamp experiments out of 272 mice, 27 were excluded on the basis of misinjection of
1169 viruses. For in vivo experiments, a total of 13 mice were excluded based on histological
1170 assessment. For histology we used the Paxinos & Franklin mouse brain atlas (The Mouse Brain,
1171 in stereotaxic coordinates, 2nd ed, 2001, Academic Press).
1172
1173 *Immunohistochemical staining for histology experiments*
1174 To stain for Channelrhodopsin, hM4DGi or control mCherry virus, tissue sections were washed
1175 in PBS (0.01 M, pH=7.4) three times for 10 minutes before incubating them for 2 hours with
1176 blocking solution (3% BSA, 0.5% Triton-X in 1x PBS). The primary antibody Rabbit Anti-RFP
1177 (Rockland, 1:1000 in blocking solution, Lot:46510) that targets mCherry, was administered to
1178 the tissue sections using ~400 ul per well. Incubation was carried out overnight at 4 degrees on
1179 a shaker to facilitate optimal antibody priming. The next day tissue sections were washed three

1180 times with PBS before applying a secondary antibody (goat-anti-Rabbit Alexa-488, Abcam,
1181 1:500, Lot:GR3375958-2, Lot:GR3442006-1). The sections were incubated with the secondary
1182 antibody for two hours before being washed in PBS again for 3 times. Finally, tissue slices were
1183 mounted on glass slides and embedded in FluorSave (Millipore, 345789, Amsterdam,
1184 Netherlands) and covered with cover glasses. The microscopy slides were allowed to air dry
1185 overnight at room temperature before being stored in a 4-degree environment to maintain
1186 sample integrity. For staining of CoChR-GFP anti-GFP antibody was used (Aves, GFP-1020,
1187 1:1000 in blocking solution) and goat-anti-chicken Alexa-568 (Abcam, 1:500) as a secondary
1188 antibody.
1189
1190 *Validation of AAV approach to label LHA_{MCH} and LHA_{OREX} cells for patch clamp*
1191 Fluorescent cells were co-filled during electrophysiology recording with internal solution and
1192 biocytin (2mg/ml). After recording, slices stayed overnight with 4% PFA at 4° C and were then
1193 transferred to PBS 0.01% NaAz. For immunolabeling, slices were first wash from NaAz with PBS
1194 solution three time for 10min in phosphate-buffered saline (PBS) then blocked 1 hour in room
1195 temperature (RT) with blocking solution (10% normal goat serum (NGS) and 5% Triton X-100 in
1196 PBS). Followed by overnight at 4°C incubation in primary antibody solution (with 1° antibodies,
1197 2% NGS and 0.4% Triton X-100 in PBS). Next day, slices were washed three time during 15 min in
1198 PBS, and incubated for three hours at RT with the 2° antibody solution (with 2° antibodies, 2%
1199 NGS and 0.4% Triton X-100 in PBS). After, slices were washed three times for 10 minutes in PBS.
1200 For the Orexin cells, first antibody used was Rabbit anti-Orexin A (1:1000, Abcam), followed by
1201 the secondary antibodies Goat anti-Rabbit 405 (1:500, Abcam) and streptavidin-AF488 (1:500).
1202 For MCH cells, slices were stained with Rabbit anti-MCH (1:1000, Sigma-Aldrich, St. Louis, MO,
1203 USA) followed by Goat anti-Rabbit 488 (1:500, Abcam) and streptavidin-AF555 (1:500). Cells
1204 were imaged with a confocal microscope.
1205
1206 *Microscopy*
1207 Slices were imaged using an EPI fluorescence microscope (Axio imager M2, Zeiss) or a confocal
1208 microscope (LSM880, Zeiss).

1209

1210 **Data analysis and statistics**

1211 Experimental data were analyzed with Ethovision (V9.0, Noldus, NL), GraphPad (v9.0, Dotmatics,
1212 UK), SPSS (v26, USA), PatchMaster (v2x78.2, HEKA, USA), Python (v3.13.5), Igor Pro-8
1213 (Wavemetrics, USA), FIJI (v2.14) and Matlab (vR2023B/vR2024B, Mathworks, USA).
1214 Experimental sample sizes were predetermined using power calculations (requiring power >0.8).
1215 These power calculations were performed together between the researchers and the local
1216 animal welfare body (AWB Utrecht). These calculations were guided by published studies, in-
1217 house expertise, and experimental pilots. Mice were randomly assigned to experimental groups.
1218 Mice or data points were not excluded from analyses unless noted. Behavioral and physiological
1219 experiments were always performed in multiple batches of animals (≥2), ensuring also internal
1220 replicability. Bar graphs are always reported and represented as mean ± SEM, with single data
1221 points plotted (single cell for electrophysiology and single animal for behavioral experiments).
1222 When statistically appropriate, One-way ANOVAs, Two-way ANOVAs, Multi-way Repeated-
1223 measures ANOVAs or t-tests were applied. Post hoc analyses were performed in case of
1224 significant omnibus ANOVA outcomes. In the event the data were not normally distributed
1225 statistical testing of group differences was performed using the Mann-Whitney U or
1226 Kolmogorov-Smirnov test. Testing was always performed two-sided with α=0.05. Complete
1227 outcome of statistical analysis is shown in Supplementary Data 1.

1228

1229 **Data availability statement**

1230 All detailed outcomes of statistical test are provided in Supplementary Data 1. Source Data are
1231 provided with this paper. Other data files are available from the corresponding author on
1232 request.

1233

1234 **Code availability statement**

1235 The location for the codes used for the analyses in the current study have been referenced in
1236 the Methods section of the manuscript.

1240 **References**

1241 1. Oliver, G. & Wardle, J. Perceived effects of stress on food choice. *Physiol Behav* 66, 511–515
1242 (1999).

1243 2. Adam, T. C. & Epel, E. S. Stress, eating and the reward system. *Physiol Behav* 91, 449–458 (2007).

1244 3. Linders, L. E. *et al.* Stress-driven potentiation of lateral hypothalamic synapses onto ventral
1245 tegmental area dopamine neurons causes increased consumption of palatable food. *Nat Commun*
1246 13, (2022).

1247 4. Dallman, M. F., Pecoraro, N. C. & La Fleur, S. E. Chronic stress and comfort foods: Self-medication
1248 and abdominal obesity. *Brain Behav Immun* 19, 275–280 (2005).

1249 5. Ulrich-lai, Y. M., Fulton, S., Wilson, M., Petrovich, G. & Rinaman, L. Stress Exposure, Food Intake,
1250 and Emotional State. 18, 381–399 (2016).

1251 6. Arnsten, A. F. T. Stress signalling pathways that impair prefrontal cortex structure and function.
1252 *Nat Rev Neurosci* 10, 410–22 (2009).

1253 7. Vander Weele, C. M., Siciliano, C. A. & Tye, K. M. Dopamine tunes prefrontal outputs to
1254 orchestrate aversive processing. *Brain Research* Preprint at
1255 https://doi.org/10.1016/j.brainres.2018.11.044 (2019).

1256 8. Balodis, I. M., Grilo, C. M. & Potenza, M. N. Neurobiological features of binge eating disorder. *CNS*
1257 *Spectrums* vol. 20 557–565 Preprint at https://doi.org/10.1017/S1092852915000814 (2015).

1258 9. Val-Laillet, D. *et al.* Neuroimaging and neuromodulation approaches to study eating behavior and
1259 prevent and treat eating disorders and obesity. *Neuroimage Clin* 8, 1–31 (2015).

1260 10. Land, B. B. *et al.* Medial prefrontal D1 dopamine neurons control food intake. *Nat Neurosci* 17,
1261 248–53 (2014).

1262 11. Mena, J. D., Selleck, R. A. & Baldo, B. A. Mu-Opioid Stimulation in Rat Prefrontal Cortex Engages
1263 Hypothalamic Orexin / Hypocretin-Containing Neurons , and Reveals Dissociable Roles of Nucleus
1264 Accumbens and Hypothalamus in Cortically Driven Feeding. *The Journal of Neuroscience* 33,
1265 18540–18552 (2013).

1266 12. Reppucci, C. J. & Petrovich, G. D. Organization of connections between the amygdala, medial
1267 prefrontal cortex, and lateral hypothalamus: a single and double retrograde tracing study in rats.
1268 *Brain Struct Funct* 221, 2937–2962 (2016).

1269 13. Stuber, G. D. & Wise, R. A. Lateral hypothalamic circuits for feeding and reward. *Nat Neurosci* 19,
1270 198–205 (2016).

1271 14. Bonnavion, P., Mickelsen, L. E., Fujita, A., de Lecea, L. & Jackson, A. C. Hubs and spokes of the
1272 lateral hypothalamus: cell types, circuits and behaviour. *Journal of Physiology* 594, 6443–6462
1273 (2016).

1274 15. Rossi, M. A. Control of energy homeostasis by the lateral hypothalamic area. *Trends in*
1275 *Neurosciences* Preprint at https://doi.org/10.1016/j.tins.2023.05.010 (2023).

1276 16. Berthoud, H. R. & Münzberg, H. The lateral hypothalamus as integrator of metabolic and
1277 environmental needs: From electrical self-stimulation to opto-genetics. *Physiol Behav* 104, 29–39
1278 (2011).

1279 17. Stuber, G. D. Neurocircuits for motivation. *Science (1979)* https://www.science.org (2023).

1280 18. Mickelsen, L. E. *et al.* Single-cell transcriptomic analysis of the lateral hypothalamic area reveals
1281 molecularly distinct populations of inhibitory and excitatory neurons. *Nat Neurosci* 22, 642–656
1282 (2019).

1283 19. Barbano, M. F., Wang, H.-L., Morales, M. & Wise, R. A. Feeding and Reward Are Differentially
1284 Induced by Activating GABAergic Lateral Hypothalamic Projections to VTA. *The Journal of*
1285 *Neuroscience* 36, 2975–2985 (2016).

1286 20. Padilla-Coreano, N. *et al.* Cortical ensembles orchestrate social competition through hypothalamic
1287 outputs. *Nature* 603, 667–671 (2022).

1288 21. Clarke, R. E. *et al.* Identification of a Stress-Sensitive Anorexigenic Neurocircuit From Medial
1289 Prefrontal Cortex to Lateral Hypothalamus. *Biol Psychiatry* 93, 309–321 (2023).

1290 22. Benchenane, K., Tiesinga, P. H. & Battaglia, F. P. Oscillations in the prefrontal cortex: A gateway to
1291 memory and attention. *Current Opinion in Neurobiology* vol. 21 475–485 Preprint at
1292 https://doi.org/10.1016/j.conb.2011.01.004 (2011).

1293 23. Razzoli, M., Sanghez, V. & Bartolomucci, A. Chronic Subordination Stress Induces Hyperphagia and
1294 Disrupts Eating Behavior in Mice Modeling Binge-Eating-Like Disorder. *Front Nutr* 1, (2015).

1295 24. Linders, L. E. *et al.* Studying Synaptic Connectivity and Strength with Optogenetics and Patch-
1296 Clamp Electrophysiology. *International Journal of Molecular Sciences* vol. 23 Preprint at
1297 https://doi.org/10.3390/ijms231911612 (2022).

1298 25. Petreanu, L., Huber, D., Sobczyk, A. & Svoboda, K. Channelrhodopsin-2-assisted circuit mapping of
1299 long-range callosal projections. *Nat Neurosci* 10, 663–668 (2007).

1300 26. Kakava-Georgiadou, N. *et al.* An intersectional approach to target neural circuits with cell- and
1301 projection-type specificity: Validation in the mesolimbic dopamine system. *Front Mol Neurosci*
1302 https://doi.org/10.3389/fnmol.2019.00049 (2019) doi:10.3389/fnmol.2019.00049.

1303 27. Petreanu, L., Mao, T., Sternson, S. M. & Svoboda, K. The subcellular organization of neocortical
1304 excitatory connections. *Nature* 457, 1142–1145 (2009).

1305 28. Rossi, M. A. *et al.* Transcriptional and functional divergence in lateral hypothalamic glutamate
1306 neurons projecting to the lateral habenula and ventral tegmental area. *Neuron*
1307 https://doi.org/10.1016/j.neuron.2021.09.020 (2021) doi:10.1016/j.neuron.2021.09.020.

1308 29. Stamatakis, A. M. *et al.* Lateral Hypothalamic Area Glutamatergic Neurons and Their Projections
1309 to the Lateral Habenula Regulate Feeding and Reward. *Journal of Neuroscience* 36, 302–311
1310 (2016).

1311 30. Herman, J. P., Tasker, J. G., Ziegler, D. R. & Cullinan, W. E. Local circuit regulation of
1312 paraventricular nucleus stress integration. *Pharmacol Biochem Behav* 71, 457–468 (2002).

1313 31. Chen, L. *et al.* Glutamatergic lateral hypothalamus promotes defensive behaviors.
1314 *Neuropharmacology* 178, (2020).

1315 32. Berrios, J. *et al.* Food cue regulation of AGRP hunger neurons guides learning. *Nature* 595, 695–
1316 700 (2021).

1317 33. Nieh, E. H. *et al.* Inhibitory Input from the Lateral Hypothalamus to the Ventral Tegmental Area
1318 Disinhibits Dopamine Neurons and Promotes Behavioral Activation. *Neuron* 90, 1286–1298
1319 (2016).

1320 34. Nieh, E. H. *et al.* Decoding neural circuits that control compulsive sucrose seeking. *Cell* 160, 528–
1321 541 (2015).

1322 35. Zingg, B. *et al.* AAV-Mediated Anterograde Transsynaptic Tagging: Mapping Corticocollicular
1323 Input-Defined Neural Pathways for Defense Behaviors. *Neuron* 93, 33–47 (2017).

1324 36. DeNardo, L. A. *et al.* Temporal evolution of cortical ensembles promoting remote memory
1325 retrieval. *Nat Neurosci* 22, 460–469 (2019).

1326 37. Koutlas, I. *et al.* Characterizing and TRAPing a Social Stress-Activated Neuronal Ensemble in the
1327 Ventral Tegmental Area. *Front Behav Neurosci* 16, (2022).

1328 38. Biro, L. *et al.* Task division within the prefrontal cortex: Distinct neuron populations selectively
1329 control different aspects of aggressive behavior via the hypothalamus. *Journal of Neuroscience*
1330 38, 4065–4075 (2018).

1331 39. Dallman, M. F. Stress-induced obesity and the emotional nervous system. *Trends in Endocrinology*
1332 *and Metabolism* 21, 159–165 (2010).

1333 40. Douglass, A. M. *et al.* Acute and circadian feedforward regulation of agouti-related peptide
1334 hunger neurons ll Article Acute and circadian feedforward regulation of agouti-related peptide
1335 hunger neurons. *Cell Metab* 37, 708-722.e5 (2025).

1336 41. Chen, Y. *et al.* Sensory Detection of Food Rapidly Modulates Arcuate Feeding Circuits Article
1337 Sensory Detection of Food Rapidly Modulates Arcuate Feeding Circuits. *Cell* 160, 829–841 (2015).

1338 42. Mandelblat-cerf, Y. *et al.* Arcuate hypothalamic AgRP and putative POMC neurons show opposite
1339 changes in spiking across multiple timescales. 1–25 (2015) doi:10.7554/eLife.07122.

1340 43. Betley, J. N. *et al.* Neurons for hunger and thirst transmit a negative-valence teaching signal.
1341 https://doi.org/10.1038/nature14416 (2015) doi:10.1038/nature14416.

1342 44. Chen, C. *et al.* The dynamic state of a prefrontal–hypothalamic–midbrain circuit commands
1343 behavioral transitions. *Nat Neurosci* https://doi.org/10.1038/s41593-024-01598-3 (2024)
1344 doi:10.1038/s41593-024-01598-3.

1345 45. Sternson, S. M. & Eiselt, A. K. Three Pillars for the Neural Control of Appetite. *Annual Review of*
1346 *Physiology* vol. 79 401–423 Preprint at https://doi.org/10.1146/annurev-physiol-021115-104948
1347 (2017).

1348 46. Zupančič, M. *et al.* Brain-wide mapping of efferent projections of glutamatergic (Onecut3 +)
1349 neurons in the lateral mouse hypothalamus. *Acta Physiologica* 238, (2023).

1350 47. Krishnan, V. *et al.* Molecular Adaptations Underlying Susceptibility and Resistance to Social Defeat
1351 in Brain Reward Regions. *Cell* 131, 391–404 (2007).

1352 48. Li, H. *et al.* Discrete prefrontal neuronal circuits determine repeated stress-induced behavioral
1353 phenotypes in male mice. *Neuron* 112, 786-804.e8 (2024).

1354 49. Vong, L. *et al.* Leptin Action on GABAergic Neurons Prevents Obesity and Reduces Inhibitory Tone
1355 to POMC Neurons. *Neuron* 71, 142–154 (2011).

1356 50. Voigts, J., Siegle, J. H., Pritchett, D. L. & Moore, C. I. The flexDrive: an ultra-light implant for optical
1357 control and highly parallel chronic recording of neuronal ensembles in freely moving mice. *Front*
1358 *Syst Neurosci* 7, (2013).

1359 51. Siegle, J. H. *et al.* Open Ephys: an open-source, plugin-based platform for multichannel
1360 electrophysiology. *J Neural Eng* 14, 045003 (2017).

1361 52. Ludwig, K. A. *et al.* Using a Common Average Reference to Improve Cortical Neuron Recordings
1362 From Microelectrode Arrays. *J Neurophysiol* 101, 1679–1689 (2009).

1363 53. Kvitsiani, D. *et al.* Distinct behavioural and network correlates of two interneuron types in
1364 prefrontal cortex. *Nature* 498, 363–366 (2013).

1365 54. Schmitzer-Torbert, N., Jackson, J., Henze, D., Harris, K. & Redish, A. D. Quantitative measures of
1366 cluster quality for use in extracellular recordings. *Neuroscience* 131, 1–11 (2005).

1367 55. Terra, H. *et al.* Prefrontal Cortical Projection Neurons Targeting Dorsomedial Striatum Control
1368 Behavioral Inhibition. *Current Biology* 30, 4188-4200.e5 (2020).

1369 56. Burgos-Robles, A. *et al.* Amygdala inputs to prefrontal cortex guide behavior amid conflicting cues
1370 of reward and punishment. *Nat Neurosci* 20, 824–835 (2017).

1371 57. Van Eenige, R. *et al.* RandoMice, a novel, user-friendly randomization tool in animal research.
1372 *PLoS One* 15, 2–9 (2020).

1373

1374

Acknowledgements

We thank Fabien Ducrocq, Salvatore Lecca, Manuel Mameli, and the entire Meye Lab for discussions and critical reading of the manuscript. We thank Zoë Bor and Luc Sangers for assistance in analysis, Jaimie Hak and Simone Duis for assistance with surgeries, Maarten Werkman and Doortje Knobbe for assistance with systemic injections, and Nicky van Kronenburg for assistance in mouse breedings. This work was supported by (to FJM) the ERC under the European Union's Horizon 2020 research and innovation programme (grant agreement 804089; ReCoDE), the NWO VIDI grant 203.102, and partially by the NWO Gravitation project BRAINSCAPES: A Roadmap from Neurogenetics to Neurobiology (024.004.012) and a Marie-Curie Individual Fellowship (CoMPOSE, grant agreement 898036) to RBP.

Author contributions

LFS performed and analysed all *ex vivo* electrophysiological recordings. KLK performed the fiber photometric recordings, together with LFS. LFS performed and analysed the following behavioral experiments: opto-stimulation of LHA_{VGLUT2}-Peri-PVN, opto-stimulation of mPFC-LHA_{VGLUT2} combining with chemogenetic inhibition, opto-stimulation of mPFC TRAP ensemble and restraint stress exposure. For these experiments LFS was further supported by FJM, WD and DR. RBP performed and analysed all other behavioral experiments, supported by AACB, ASJN and RH. RBP performed and analysed *in vivo* electrophysiological recordings. LFS, RBP, IW-D and MCML performed stereotactic surgeries. FJM designed the study with RBP and LFS. FJM wrote the manuscript with LS, RAHA, RBP and the help of all other authors.

Competing interests statement

The authors declare no competing interests.

1402

1403 **Figures and Figure legends**

1404

1405

1406

1407 **Figure 1. Frequency-dependent increase of palatable food intake by mPFC-LHA pathway**
1408 **stimulation. (A)** Experimental timeline and viral and optogenetic strategy to manipulate mPFC-
1409 LHA pathway activity. **(B)** Left: Histological verification of CoChR-GFP expression in mPFC
1410 subterritories cingulate cortex (Cg1), Prelimbic cortex (PrL) and infralimbic cortex (IL) (top), and
1411 optic fiber location in LHA (bottom, white arrows indicate end of optic fibers). Right: mPFC
1412 axons in LHA. **(C)** Schematic of behavioral paradigm. Food intake on the test day was measured
1413 against three baseline days. On stimulation day mPFC-LHA pathway was stimulated in blocks of
1414 10 minutes alternated by non-stimulated blocks. **(D)** Bar graphs showing fat consumption
1415 normalized to intake of the first three baseline days for different stimulation frequencies. Plots
1416 show fat intake on baseline day 3, stimulation day and post-stimulation day. For 1Hz: YFP n=19,
1417 CoChR n=19, Two-way RM ANOVA, Day-Virus interaction $F(2,72)=1.34$, $p=0.18$). For 5Hz: YFP
1418 n=19, CoChR n=19, Two-way RM ANOVA, Day-Virus interaction, $F(2,72)=3.37$, $p=0.04$. Opsin-
1419 expressing mice on stimulation day compared to baseline (YFP n=19, CoChR n=19, Sidák's
1420 multiple comparison test, $p=0.007$). **(E)** Bar graphs of video-based analysis of feeding bouts over
1421 the hour without or with mPFC-LHA optogenetic stimulation. Effect of 1 Hz (left): YFP n=13,
1422 CoChR n=13, Two-way RM ANOVA, Interaction Time-Virus, $F(5,120)=0.17$, $p=0.95$). Effect of 5 Hz
1423 (right): YFP n=12, CoChR n=12, Two-way RM ANOVA, Interaction Time-Virus, $F(5,110)=2.83$,
1424 $p=0.037$. Sidák's multiple comparison test 30-40m, YFP vs CoChR, $p=0.038$ and 50-60m, $p=0.013$.
1425 **(F)** Bar graphs for effect of mPFC-LHA stimulation on feeding bouts quantified according to laser
1426 ON and OFF blocks. For 1Hz: YFP n=13, CoChR n=13, Two-way RM ANOVA, Interaction Time-
1427 Virus, $F(1,24)=0.06$. For 5Hz: YFP n=12, CoChR n=12, Two-way RM ANOVA, Interaction Time-
1428 Virus, $F(1,22)=7.64$, $p=0.011$, Sidák's multiple comparison test ON blocks YFP vs CoChR,
1429 $p=0.003$).
1430 In bar graph (D, E, F) the superimposed points represent individual animals and error bars
1431 represent their SEMs. *= $p<0.05$; **= $p<0.01$.

1432

1433 **Figure 2. mPFC-LHA neuronal activity is diversely modulated by social stress. (A)** Viral strategy
1434 and implantation of optrodes (i.e. 32 electrode wires and an optic fiber) for extracellular
1435 recordings of opto-identified LHA-projecting mPFC neurons. **(B)** Left: Histological verification of
1436 placement of electrode tip in between opsin-expressing mPFC neurons projecting to LHA. Tip of
1437 optrodes indicated with a yellow arrow. Right: Histology of LHA targeting with the Cav2-Cre
1438 retrograde virus. Anatomical reference point: fmi=forceps minor of the corpus callosum,
1439 EPN=entopeduncular nucleus, f=fornix. **(C)** Optogenetic-assisted identification of mPFC
1440 pyramidal neurons projecting to the LHA. Neurons were classified as being opto-tagged if they
1441 showed a significant increase in firing rate after light stimulation compared to baseline using the
1442 SALT-test (see methods for test, and see Suppl. Datafile for individual neuron SALT p values). (**D**)
1443 Behavioral paradigm to record mPFC-LHA cellular activity during social stress. **(E)** Bidirectional
1444 modulation of distinct mPFC-LHA neurons by social stress. Top: histograms of single cell
1445 examples (10s bins comparing 180 seconds right before and after fight onset, Wilcoxon signed-
1446 rank test, $p<0.05$). Bottom: Histograms showing group averages (n=26 opto-identified mPFC-
1447 LHA cells from 12 mice; mPFC-LHA cells that decrease firing n=13 cells; mPFC-LHA cells that
1448 increase firing n=7 cells). Dotted line indicates the average length of the stress exposure. Error
1449 bars in histograms indicate SEMs across neurons. **(F)** Pie chart showing mPFC-LHA neurons
1450 which were significantly modulated by, or not responsive to, the social stress experience (n=26
1451 opto-tagged mPFC-LHA cells from 12 mice). *= $p<0.05$.

1452

1453 **Figure 3. mPFC-LHA neuronal activity is required for stress-driven over intake of fat and the**
1454 **pathway is modulated by feeding**. **(A)** Viral strategy to make mPFC-LHA neurons susceptible to
1455 chemogenetic inhibition. **(B)** Histology of injection sites of CAV2-Cre in the LHA using red beads,
1456 and of hM4Di-mCherry expression in mPFC subterritories PrL and IL (antibody for green
1457 fluorescence). Anatomical reference point: cp=cerebral peduncle. **(C)** Timeline of the stress-
1458 driven food intake experiment with chemogenetic mPFC-LHA manipulation. **(D)** Effect of
1459 chemogenetic inhibition of mPFC-LHA on food intake. Delta food intake during test day (Day +3)
1460 compared to the baseline session (Day -5). Left: Effect on (stress-driven) fat intake (mCherry-
1461 Control n=13, hM4Di-control n=13, mCherry-Stress n=14, hM4Di-Stress n=14, Two-way ANOVA,
1462 Treatment-Virus interaction, F(1,50)=4.69, p=0.035, Sidáks multiple comparison test mCherry-
1463 control vs mCherry-Stress, p=0.015, hM4Di-control vs hM4Di-Stress, p>0.99, mCherry-control vs
1464 hM4Di-control, p=0.61). Right: Effect on chow intake (mCherry-Control n=13, hM4Di-control
1465 n=13, mCherry-Stress n=14, hM4Di-Stress n=14, Two-way ANOVA, Treatment-Virus interaction,
1466 F(1,50)=0.07, p=0.79). **(E)** Schematic and timeline for fiber photometric measurements from
1467 mPFC neurons projecting to LHA. **(F)** Line graph showing average calcium response time course
1468 of the mPFC-LHA population to social stress. Dotted lines show SEMs, based on different mice
1469 (n=8). **(G)** Left: Bar graph quantifying the peaks after social stress. N=8 mice, Wilcoxon matched
1470 pairs, W=36, p=0.008. Right: Bar graph quantifying the dips after social stress. N=8 mice,
1471 Wilcoxon matched pairs, W=34, p=0.016. **(H)** Line graph showing time courses of dips in mPFC-
1472 LHA pathway during onset of food intake in either control context (n=8 mice) or after 2 days of
1473 social stress (n=8 mice). Shaded areas show SEMs, based on different animals. **(I)** As (H) but for
1474 offset of fat interaction. **(J)** Bar graph quantifications of dips with respect to baseline both in
1475 control (n=8) or after social stress (n=8). Two-Way ANOVA, Stress-Time interaction,
1476 F(1,14)=0.53, p=0.48. Main effect Time (F1,14)=21.01, p=0.0004. Fisher's LSD multiple
1477 comparison control baseline vs fat contact t(14)=3.754, p=0.0021, stress baseline vs fat contact
1478 t(14)=2.729, p=0.0163. In bar graph (D, G, J) superimposed points represent individual animals
1479 and error bars represent SEMs. *= p<0.05; **= p<0.01.

1480 **Figure 4. mPFC sends direct excitatory projections to multiple LHA neuronal populations. (A)**
1481 Schematic of the viral strategies to identify LHA populations and to express an opsin in mPFC.
1482 **(B)** Left: Representative image of the viral expression in mPFC (in green) and in LHA cell types (in
1483 red) in coronal slices. Scale bar 200µm. Right: Representative image of the different LHA
1484 neuronal subsets (red) during patch clamp experiments. Scale bar 10µm. **(C)** Quantifications of
1485 extent of synaptic connectivity between mPFC and different LHA subpopulations. From left to
1486 right, cumulative probability plots of opto-evoked AMPAR amplitudes, after mPFC input
1487 stimulation, in LHA_{VGAT} (n cells = 23 from 9 mice), LHA_{Vglut2} (n cells = 30 from 10 mice), LHA_{MCH} (n
1488 cells = 31 from 10 mice) and LHA_{OREX} (n cells= 38 from 10 mice) populations. Alongside are pie
1489 chart representations of the proportion of LHA cells connected to mPFC (n VGAT cells= 27, n
1490 Vglut2 cells= 31, n MCH cells= 32 and n Orexin cells= 38). For the voltage-clamp trace examples
1491 within the graph, blue rectangles represent 1 ms of opto-stimulation. **(D)** Left: Example timeline
1492 of EPSCs in an LHA_{VGLUT2} cell during baseline, during application of TTX and with further addition
1493 of 4-AP. SEMs represent variation in binned sweeps (bins of 60 seconds). Right: Bar graph
1494 showing the percentage of connectivity to mPFC for the 4 LHA populations in presence of 4AP +
1495 TTX (n VGAT cells= 10, 1 mouse, n Vglut2 cells= 11, 1 mouse, n MCH cells= 9, 2 mice and n
1496 Orexin cells= 12, 2 mice), showing a high monosynaptic connectivity that was similar across
1497 cellular populations (Pearson Chi-Square test, $\chi2=3.166$, $p = 0.367$).

1498

Figure 5. Social stress drives divergent plasticity at mPFC synapses onto distinct LHA_{VGLUT2} neuronal subsets. (A) Cumulative probability plots of opto-evoked AMPARs in neurons from distinct LHA subpopulations for control (black) and stress (red) conditions, with representative example trace insets. Top: mPFC-LHA_{VGLUT2} synapses (n control=30, 10 mice, n stress=35, 11 mice; Mann-Whitney test, U=342, p=0.0152). Middle: mPFC-LHA_{VGAT} synapses (n control=23, 8 mice, n stress= 21, 9 mice; Mann-Whitney test, U=232, p=0.8341). Bottom: mPFC-LHA_{OREX} population (n control=37, 10 mice, n stress=35, 9 mice; Mann-Whitney test, U=582, p=0.4663). **(B)** Example traces (left) and bar graphs (right) for paired pulse ratios (PPRs) at mPFC synapses onto distinct LHA subpopulations, for control (black) and stress (red) conditions. PPRs at distinct inter pulse intervals (IPIs) of 60, 100 and 200 ms are shown. Top: mPFC- LHA_{VGLUT2} synapses (n control=19, 10 mice, n stress= 20, 11 mice; two-way RM ANOVA, Main effect of group, F(1,37)=4.55, p=0.04). Middle: mPFC-LHA_{VGAT} synapses (n control= 16, 7 mice, n stress= 18, 9 mice; Two-way RM ANOVA, Main effect of group, F(1,32)=0.160, p=0.691). Bottom: mPFC-LHA_{OREX} synapses (n control= 32, 10 mice, n stress= 34, 9 mice; Two-way RM ANOVA, Main effect of group, F(1,64)=1.752, p=0.19). **(C)** Schematic and experimental timeline for patch clamp recordings of mPFC synaptic inputs on LHA_{VGLUT2} cells with distinct downstream targets. **(D)** Representative images of retrograde targeting VTA, Peri-PVN or LHb. Scale bar 200µm. **(E)** Left: example traces for mPFC-LHA_{VGLUT2}-Peri-PVN synapses in control (black) and stress (red) conditions during 100 ms IPI. Right: Bar graph representation of PPRs (n control= 14, 5 mice, n stress= 12, 4 mice; two-way RM ANOVA, Main effect of group, F(1,24)=5.975, p=0.022). **(F)** As E, but for mPFC-LHA_{VGLUT2}-LHb synapses (n control= 9, 4 mice, n stress= 7, 4 mice; Two-way RM ANOVA, Main effect of group, F(1,14)=0.099, p=0.758). Scale bar 200µm. **(G)** As E, but for mPFC-LHA_{VGLUT2}-VTA synapses (n control= 27, 9 mice, n stress=17, 6 mice; Two-way RM ANOVA, Main effect of group, F(1,42)=7.13, p= 0.011). In bar graphs (B, E-G) superimposed points represent individual neurons and error bars represent their SEMs. *= p<0.05.

1527 **Figure 6. *In vivo* mPFC-LHA stimulation further increases fat intake after stress, by preventing**
1528 **a decline of interest in the fat. (A)** Experimental strategy to stimulate mPFC-LHA pathway in
1529 control and stressed conditions. **(B)** Histological verification of mPFC axonal processes in LHA.
1530 **(C)** Bar graphs showing fat intake over the 2 hours for experimental groups (Control n=27, Stress
1531 n=23 Stress; Two-way ANOVA, main effect treatment, F(1,46)=15, p=0.0003). Main effect
1532 stimulation F(1,46)=10.38, p=0.002). Stress plus mPFC-LHA stimulation resulted in largest
1533 consumption of fat (Sidák's multiple comparison tests: Stress-5Hz vs Stress-Mock, t(46)=3.27,
1534 p=0.01; Stress-5Hz vs Ctrl-5Hz, t(46)=3.78, p=0.003). **(D)** Cumulative plots for feeding bouts over
1535 the course of two hours for mock and 5Hz stimulation (Mock Stim: Control n=14, Stress n=12;
1536 5Hz Stim: Control n=13, 5 Hz n=11). **(E)** Bar graph quantification of feeding bouts for non-
1537 stimulated mice during the Binge and Post-binge phase for controls (n=12) and stressed mice
1538 (n=14). Binge phase (0-20 min): unpaired t-test, t(24)=3.49, p=0.002. Post-binge phase (20-120
1539 min): Mann-Whitney test, U(24)=15, p=0.0001. **(F)** Bar graph quantification of 5Hz stimulation
1540 effect on feeding bouts during the Binge phase (Control Mock n=14, Control 5Hz n=13, Stress
1541 Mock n=12, Stress 5Hz n=11; Two-Way ANOVA, interaction Stimulation- Treatment,
1542 F(1,46)=0.52, p=0.48), and the Post-Binge phase (Control Mock n=14, Control 5Hz n=13, Stress
1543 Mock n=12, Stress 5Hz n=11, Two-Way ANOVA, Stimulation-Treatment interaction,
1544 F(1,46)=4.05, p=0.05, Sidák's multiple comparison test mock stim vs 5Hz in stressed condition,
1545 t(46)=4, p=0.0004). **(G)** Bar graph of data in F normalized to total feeding bouts indicating
1546 persistence of fat consumption beyond the Binge phase (Two-Way ANOVA, interaction
1547 Stimulation-Treatment, F(1,46)=9.47, p=0.004, Sidák's multiple comparison test Mock stim vs
1548 5Hz in stressed condition, t(46)=4.825, p=0.0001). In bar graphs (C, E-G) the superimposed
1549 points represent individual animals and error bars represent their SEMs. *= p<0.05; **= p<0.01;
1550 ***=p<0.001.

1551

1552

1553 **Figure 7. LHA glutamatergic neurons are important mediators of the effects of stress on food**
1554 **intake. (A)** Schematic for viral targeting and experimental timeline. **(B)** Histological verification
1555 of targeting LHA with chemogenetic actuator (red). **(C)** Bar graph of fat intake over 2 hours
1556 (Vehicle-control n=6, Vehicle-stress n=7, CNO-control n=6, CNO-stress n=6; Two Way ANOVA,
1557 Stress-CNO interaction $F(1,21)=4.408$, $p=0.048$. Sidak post hoc comparisons vehicle-control
1558 versus vehicle-stress, $p=0.034$; CNO-control versus CNO-stress, $p=0.99$; Vehicle-stress versus
1559 CNO-stress, $p=0.03$. (**D**) Schematic and timeline for TRAPing mPFC ensemble during social stress
1560 ($mPFC_{SOCIAL\ STRESS}$) or during novel mouse exposure ($mPFC_{NOVEL\ MOUSE}$). (**E**) Left: Representative
1561 image of opsin expression after TRAP recombination after an acute stress episode in mPFC.
1562 Scale bar 200µm. Right: Representative images of viral fluorophore expression for co-labeling
1563 distinct LHA populations. Top: MCH (red) and VGAT (green) neurons, Bottom: Orexin (red) and
1564 Vglut2 (green) neurons. **(F)** Schematic approach of patch recordings from specific LHA neuron
1565 types in brain slices, while optogenetically stimulating mPFC ensemble axons. (**G)**
1566 Representative examples of averaged $mPFC_{SOCIAL\ STRESS}$ opto-evoked EPSC in LHA_{VGAT} (purple),
1567 LHA_{VGLUT2} (blue), LHA_{MCH} (green) and LHA_{OREX} (yellow) neurons. Blue rectangle indicates 1ms
1568 opto-stimulation. **(H)** Pie charts for connectivity of $mPFC_{SOCIAL\ STRESS}$ and $mPFC_{NOVEL\ MOUSE}$
1569 ensembles with distinct LHA populations (VGAT, Vglut2, MCH and Orexin). $mPFC_{SOCIAL\ STRESS}$
1570 ensemble connected more with glutamatergic than GABA LHA subtypes (n-VGAT =31, 6 mice; n-
1571 Vglut2=49, 11 mice; n-MCH=15, 5 mice; n-Orexin=23, 8 mice; Pearson Chi-Square test, $Z=21$,
1572 $p=0.0007$). $mPFC_{SOCIAL\ STRESS}$ ensemble connected more to LHA_{VGLUT2} (Pearson Chi-Square test,
1573 $Z=7.14$, $p=0.008$); and LHA_{OREX} neurons (Pearson Chi-Square test, $Z=8.37$, $p=0.004$) than did the
1574 $mPFC_{NOVEL\ MOUSE}$ ensemble. **(I)** Schematics for approach and timeline for ensemble pathway
1575 stimulation in the 2-choice food assay. **(J)** Histological validation of the opsin in mPFC ensemble
1576 somata (left) and axons in LHA (right). **(K)** Bar graph quantification of fat intake over the 2 hours
1577 for $mPFC_{SOCIAL\ STRESS}$ (n=7) and $mPFC_{NOVEL\ MOUSE}$ (n=7) ensemble projection to LHA, as a delta from
1578 baseline. Mann Whitney $U=7.5$, $p=0.027$. In bar graphs (C and K) the superimposed points
1579 represent individual animals and error bars represent their SEMs. *= $p<0.05$; **= $p<0.01$;
1580 ***=$p<0.001$.

1581

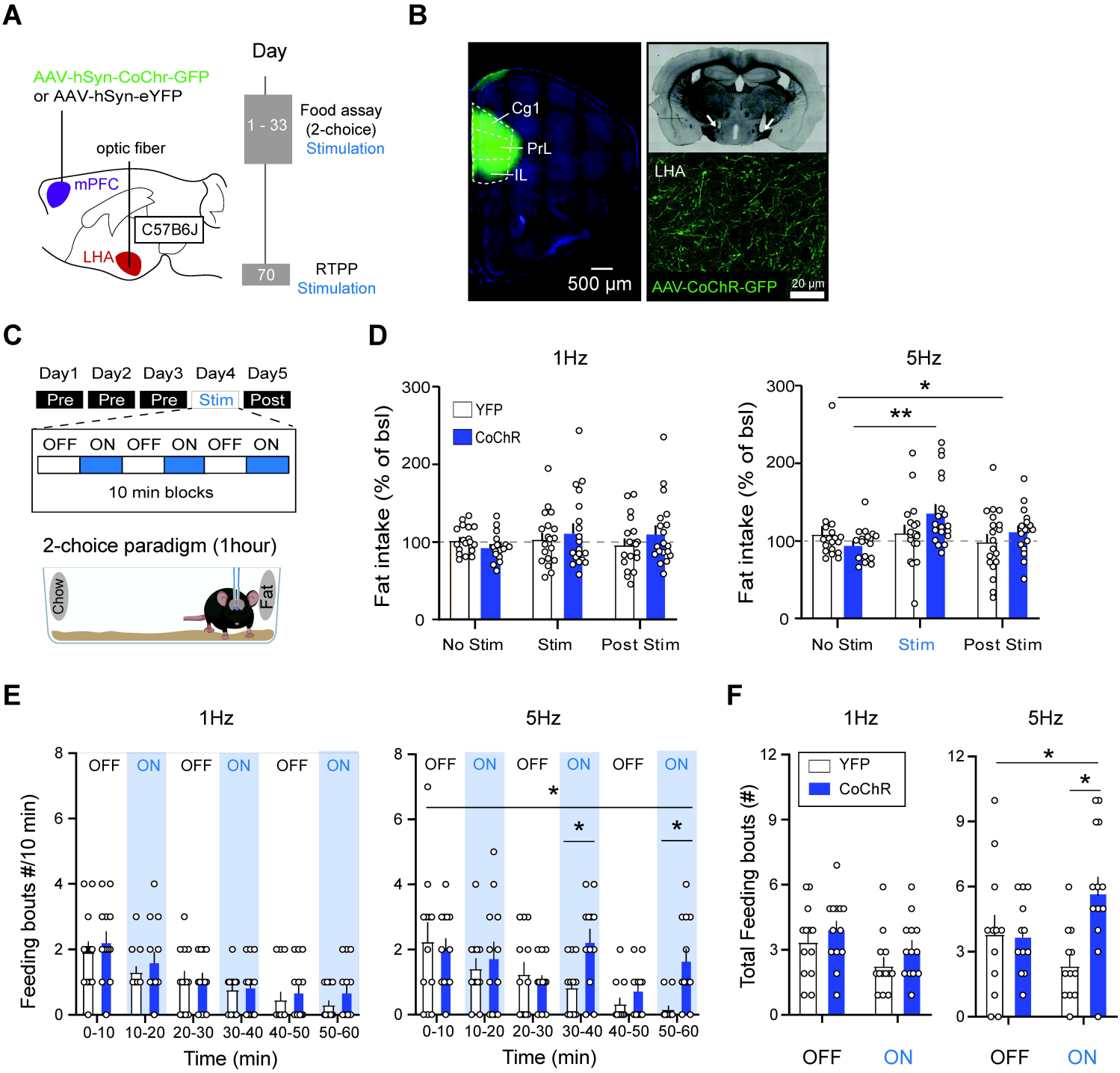
A
AAV-hSyn-CoChr-GFP
or AAV-hSyn-eYFP
optic fiber
mPFC
C57B6J
LHA
Day
1 - 33
Food assay
(2-choice)
Stimulation
70
RTPP
Stimulation
B
Cg1
PrL
IL
500 µm
LHA
AAV-CoChR-GFP
20 µm
C
Day1 Day2 Day3 Day4 Day5
Pre Pre Pre Stim Post
OFF ON OFF ON OFF ON
10 min blocks
2-choice paradigm (1hour)
Chow
Fat
D
1Hz
5Hz
YFP
CoChR
Fat intake (% of bsl)
No Stim
Stim
Post Stim
E
1Hz
5Hz
OFF
ON
Feeding bouts #/10 min)
0-10
10-20
20-30
30-40
40-50
50-60
Time (min)
F
1Hz
5Hz
YFP
CoChR
Total Feeding bouts (#)
OFF
ON

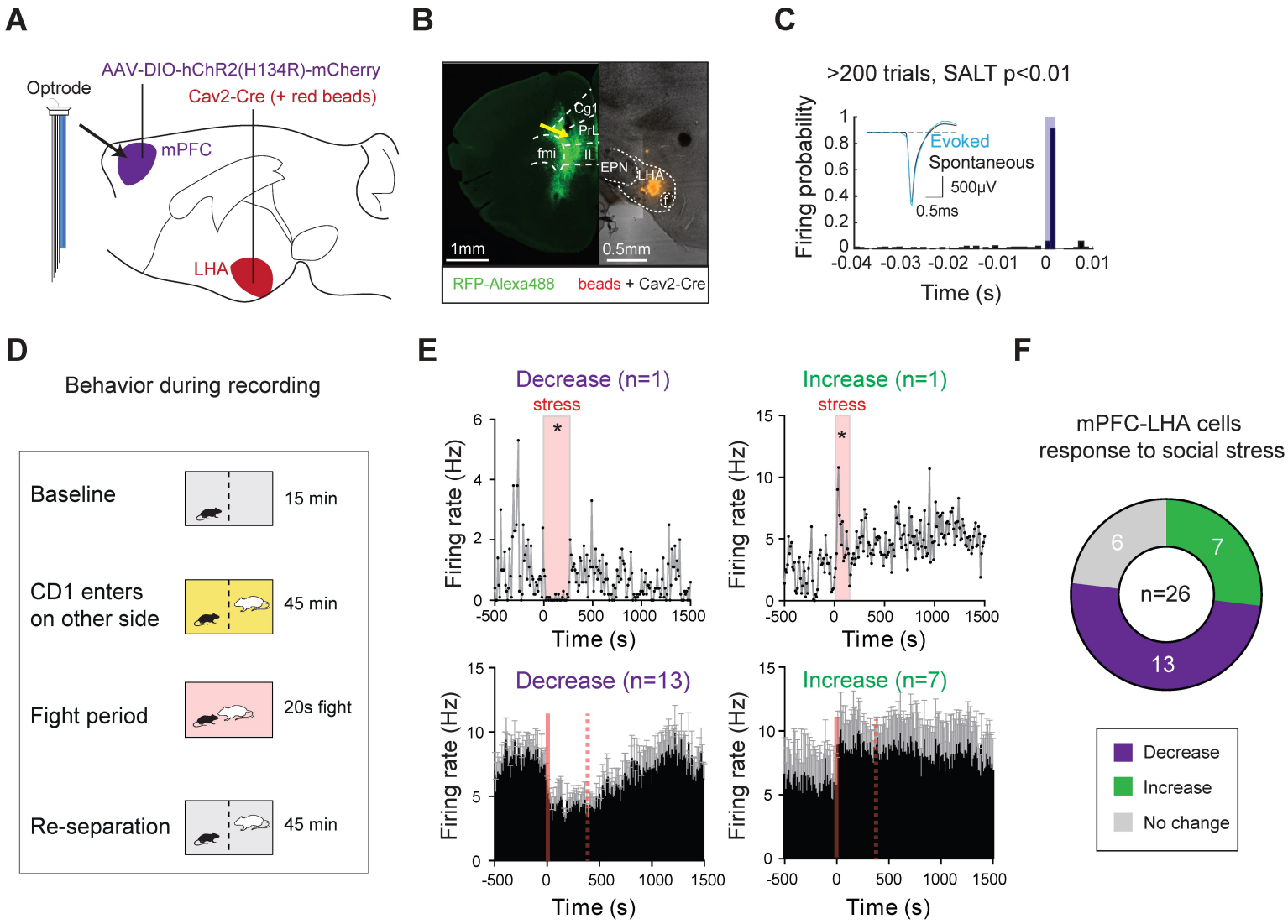
A
Optrode
AAV-DIO-hChR2(H134R)-mCherry
Cav2-Cre (+ red beads)
mPFC
LHA
B
Cg1
PrL
fmi
IL
EPN
LHA
f
1mm
0.5mm
RFP-Alexa488
beads + Cav2-Cre
C
>200 trials, SALT p<0.01
Firing probability
Evoked
Spontaneous
500μV
0.5ms
Time (s)
D
Behavior during recording
Baseline
15 min
CD1 enters on other side
45 min
Fight period
20s fight
Re-separation
45 min
E
Decrease (n=1)
Increase (n=1)
stress
Firing rate (Hz)
Time (s)
Decrease (n=13)
Increase (n=7)
F
mPFC-LHA cells response to social stress
n=26
6
7
13
Decrease
Increase
No change

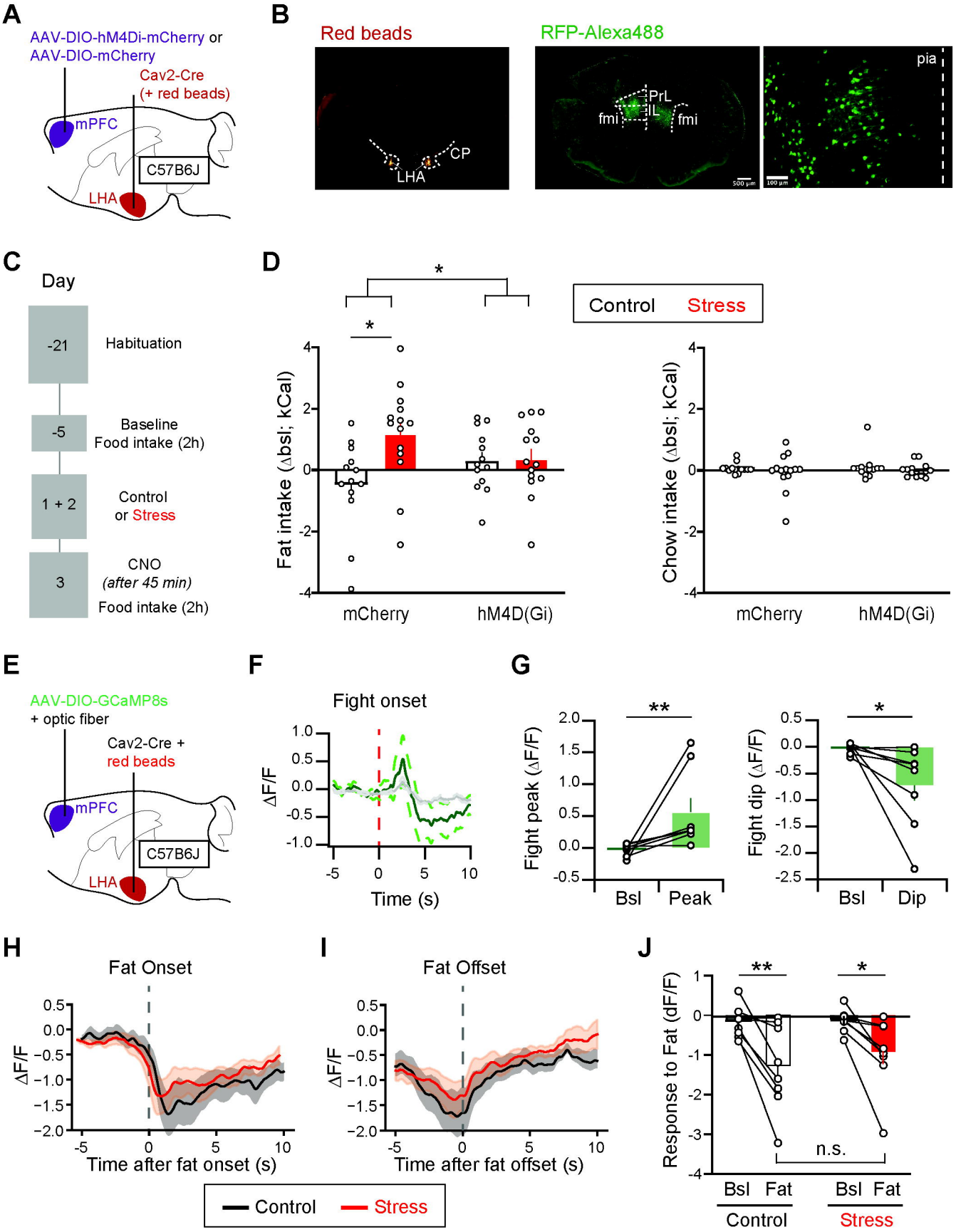
A
AAV-DIO-hM4Di-mCherry or
AAV-DIO-mCherry
Cav2-Cre
(+ red beads)
mPFC
C57B6J
LHA
B
Red beads
RFP-Alexa488
CP
LHA
PrL
IL
fmi
fmi
pia
C
Day
-21
Habituation
-5
Baseline
Food intake (2h)
1 + 2
Control
or Stress
3
CNO
(after 45 min)
Food intake (2h)
D
Control
Stress
Fat intake (Δbsl; kCal)
Chow intake (Δbsl; kCal)
mCherry
hM4D(Gi)
E
AAV-DIO-GCaMP8s
+ optic fiber
Cav2-Cre +
red beads
mPFC
C57B6J
LHA
F
Fight onset
ΔF/F
Time (s)
G
Fight peak (ΔF/F)
Bsl
Peak
Fight dip (ΔF/F)
Bsl
Dip
H
Fat Onset
ΔF/F
Time after fat onset (s)
I
Fat Offset
ΔF/F
Time after fat offset (s)
Control
Stress
J
Response to Fat (dF/F)
n.s.
Bsl
Fat
Control
Bsl
Fat
Stress

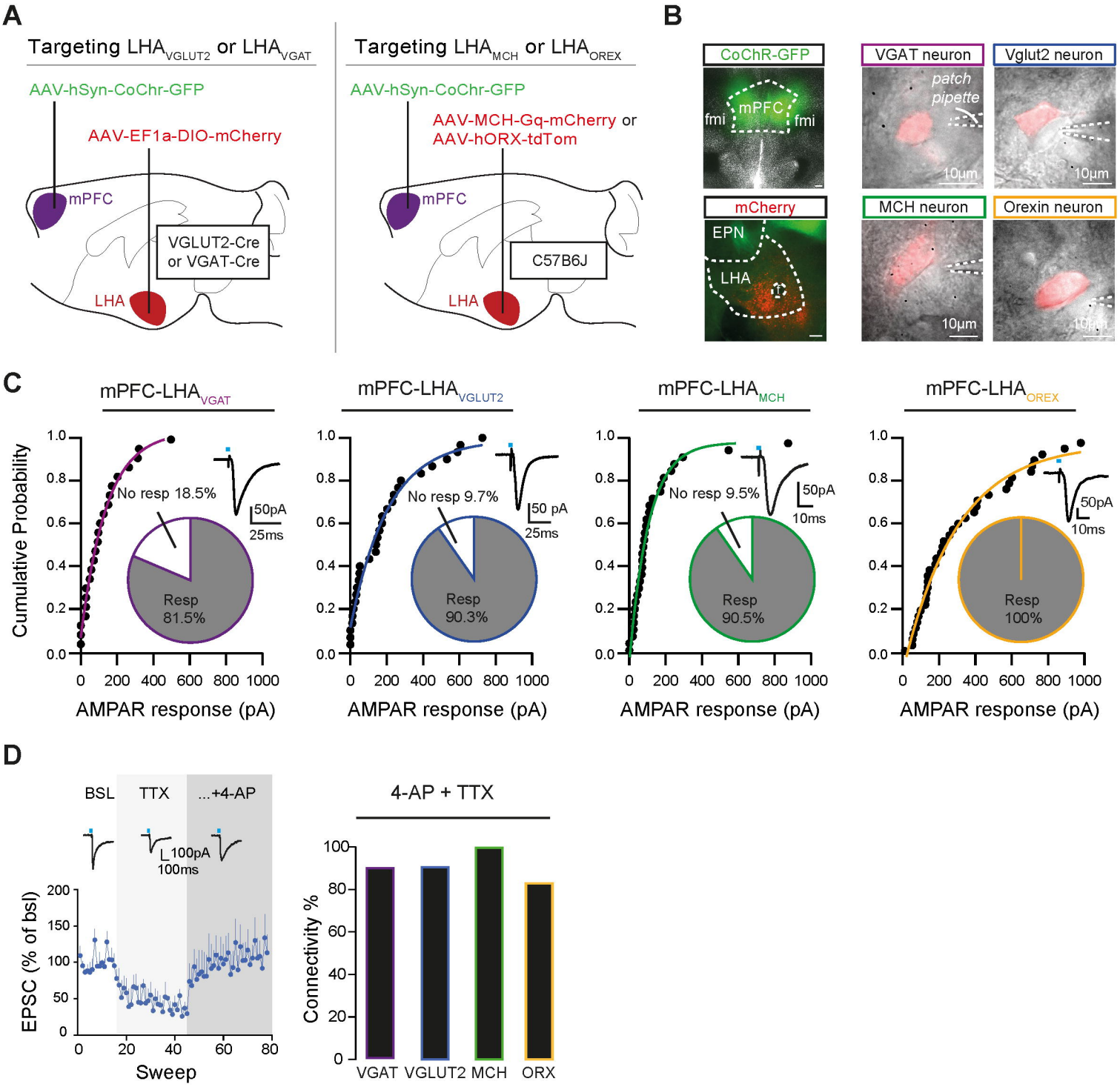
A
Targeting LHA$_{VGLUT2}$ or LHA$_{VGAT}$
AAV-hSyn-CoChr-GFP
AAV-EF1a-DIO-mCherry
mPFC
VGLUT2-Cre
or VGAT-Cre
LHA
Targeting LHA$_{MCH}$ or LHA$_{OREX}$
AAV-hSyn-CoChr-GFP
AAV-MCH-Gq-mCherry or
AAV-hORX-tdTom
mPFC
C57B6J
LHA
B
CoChR-GFP
fmi
mPFC
fmi
mCherry
EPN
LHA
VGAT neuron
patch
pipette
10µm
Vglut2 neuron
10µm
MCH neuron
10µm
Orexin neuron
C
mPFC-LHA$_{VGAT}$
Cumulative Probability
No resp 18.5%
50pA
25ms
Resp
81.5%
AMPAR response (pA)
mPFC-LHA$_{VGLUT2}$
No resp 9.7%
50 pA
25ms
Resp
90.3%
AMPAR response (pA)
mPFC-LHA$_{MCH}$
No resp 9.5%
50pA
10ms
Resp
90.5%
AMPAR response (pA)
mPFC-LHA$_{OREX}$
50pA
10ms
Resp
100%
AMPAR response (pA)
D
BSL
TTX
...+4-AP
100pA
100ms
EPSC (% of bsl)
Sweep
4-AP + TTX
Connectivity %
VGAT
VGLUT2
MCH
ORX

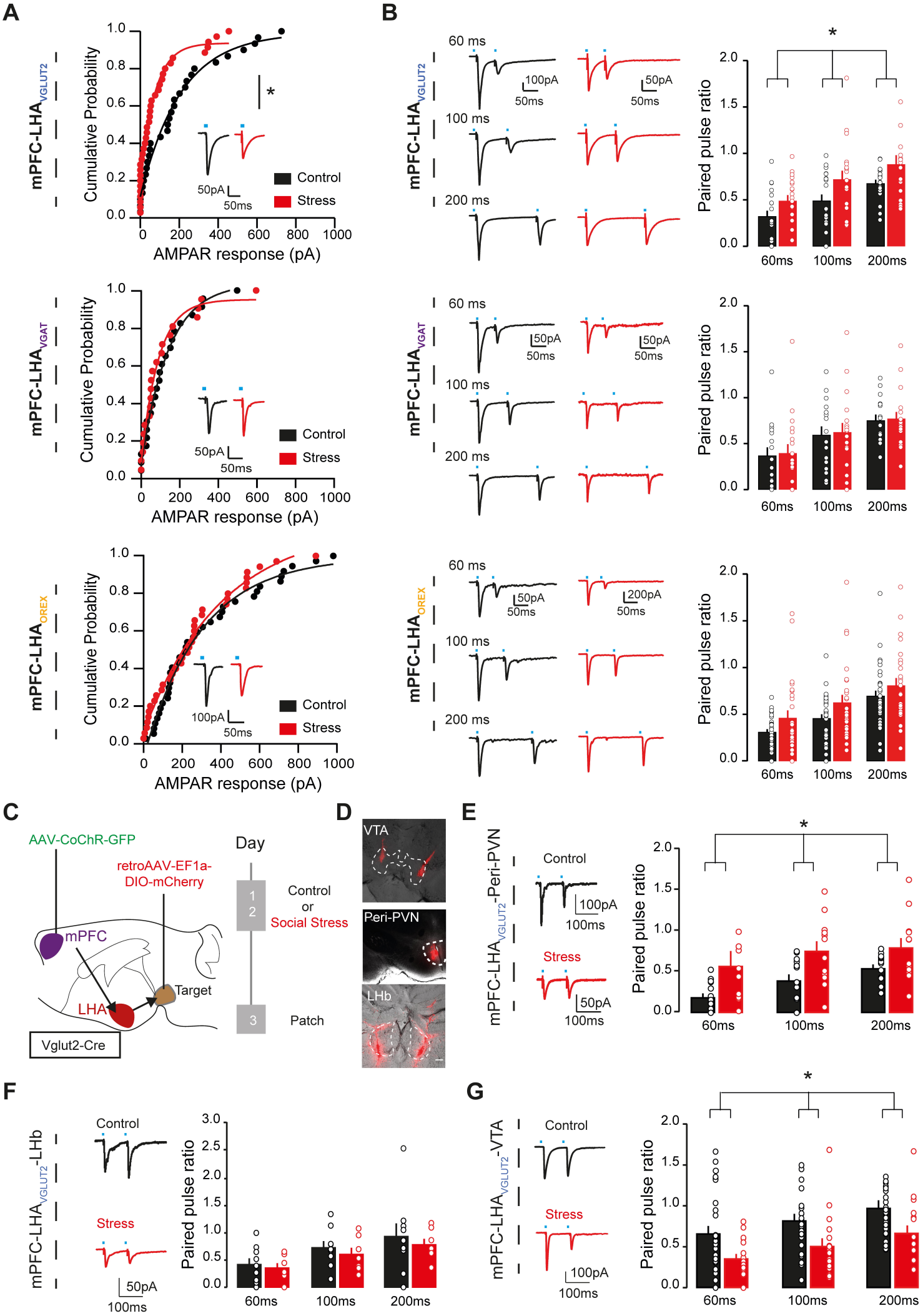
A
mPFC-LHA VGLUT2
Cumulative Probability
AMPAR response (pA)
Control
Stress
50pA
50ms
mPFC-LHA VGAT
mPFC-LHA OREX
100pA
B
60 ms
100 ms
200 ms
Paired pulse ratio
60ms
100ms
200ms
C
AAV-CoChR-GFP
retroAAV-EF1a-DIO-mCherry
mPFC
LHA
Target
Vglut2-Cre
Day
Control or Social Stress
Patch
D
VTA
Peri-PVN
LHb
E
mPFC-LHA VGLUT2-Peri-PVN
F
mPFC-LHA VGLUT2-LHb
G
mPFC-LHA VGLUT2-VTA

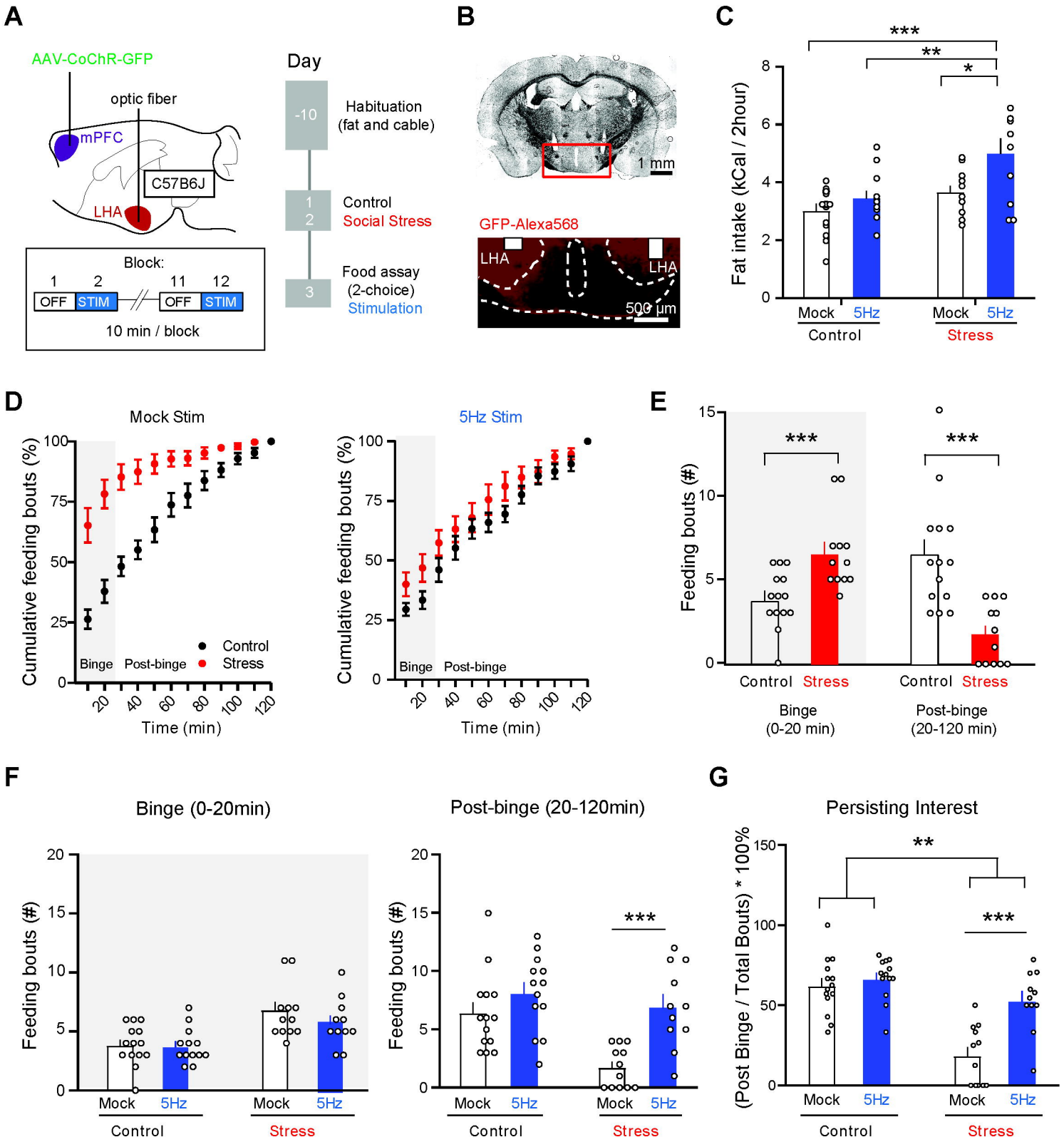
A
AAV-CoChR-GFP
optic fiber
mPFC
C57B6J
LHA
Block:
1 2 11 12
OFF STIM OFF STIM
10 min / block
Day
-10
Habituation
(fat and cable)
1
2
Control
Social Stress
3
Food assay
(2-choice)
Stimulation
B
1 mm
GFP-Alexa568
LHA
LHA
500 µm
C
Fat intake (kCal / 2hour)
Mock
5Hz
Control
Stress
D
Mock Stim
5Hz Stim
Cumulative feeding bouts (%)
Binge
Post-binge
Control
Stress
Time (min)
E
Feeding bouts (#)
Control
Stress
Binge
(0-20 min)
Post-binge
(20-120 min)
F
Binge (0-20min)
Post-binge (20-120min)
Feeding bouts (#)
Mock
5Hz
Control
Stress
G
Persisting Interest
(Post Binge / Total Bouts) * 100%
Mock
5Hz
Control
Stress

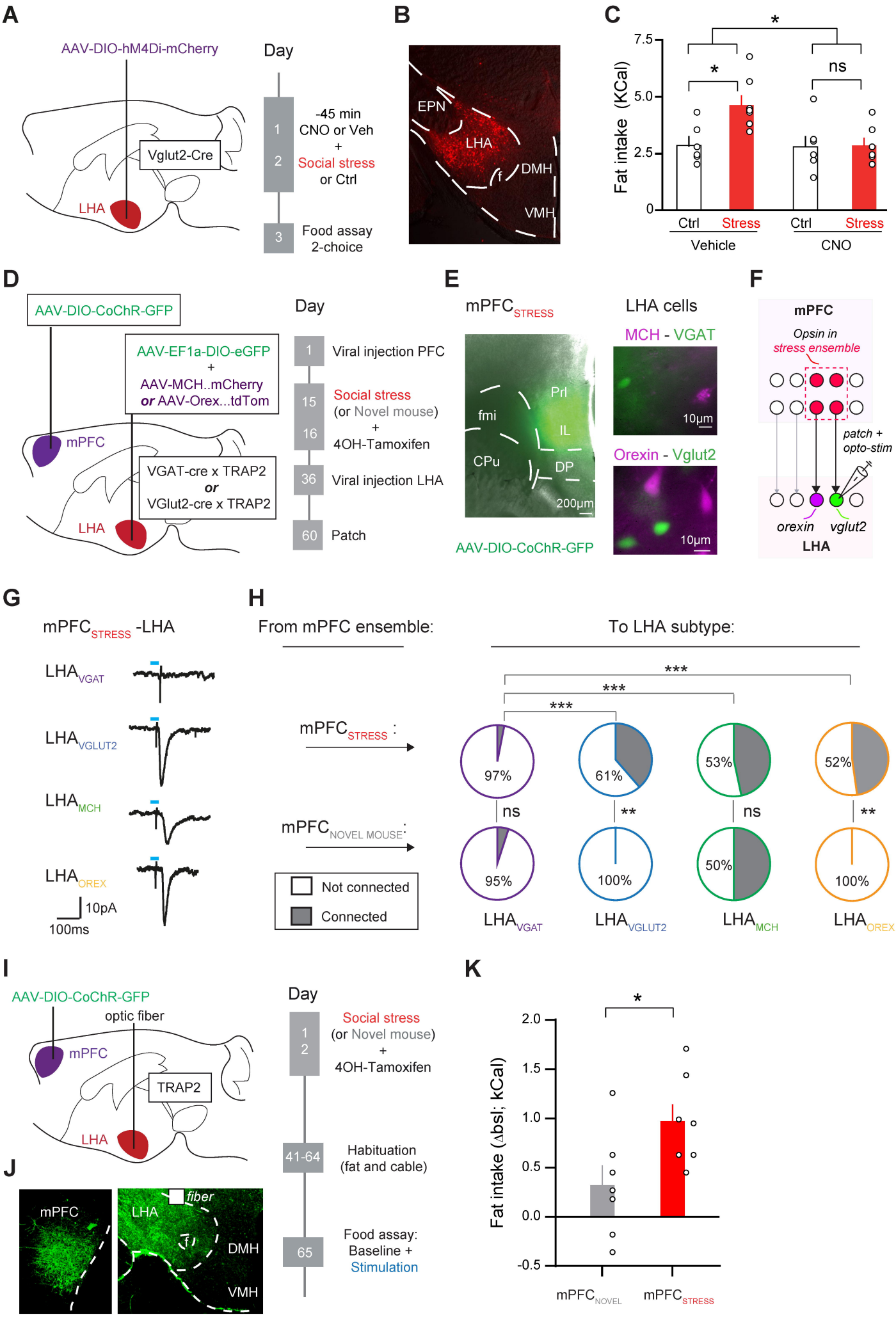
A
AAV-DIO-hM4Di-mCherry
Vglut2-Cre
LHA
Day
1
2
3
-45 min
CNO or Veh
+
Social stress
or Ctrl
Food assay
2-choice
B
EPN
LHA
f
DMH
VMH
C
Fat intake (KCal)
7.5
5.0
2.5
0
*
*
ns
Ctrl
Stress
Ctrl
Stress
Vehicle
CNO
D
AAV-DIO-CoChR-GFP
AAV-EF1a-DIO-eGFP
+
AAV-MCH..mCherry
or AAV-Orex...tdTom
mPFC
VGAT-cre x TRAP2
or
VGlut2-cre x TRAP2
LHA
Day
1
Viral injection PFC
15
16
Social stress
(or Novel mouse)
+
4OH-Tamoxifen
36
Viral injection LHA
60
Patch
E
mPFCSTRESS
fmi
Prl
IL
CPu
DP
200µm
AAV-DIO-CoChR-GFP
LHA cells
MCH - VGAT
10µm
Orexin - Vglut2
10µm
F
mPFC
Opsin in
stress ensemble
patch +
opto-stim
orexin
vglut2
LHA
G
mPFCSTRESS -LHA
LHAVGAT
LHAVGLUT2
LHAMCH
LHAOREX
10pA
100ms
H
From mPFC ensemble:
To LHA subtype:
mPFCSTRESS :
mPFCNOVEL MOUSE:
Not connected
Connected
***
***
***
97%
61%
53%
52%
ns
**
ns
**
95%
100%
50%
100%
LHAVGAT
LHAVGLUT2
LHAMCH
LHAOREX
I
AAV-DIO-CoChR-GFP
optic fiber
mPFC
TRAP2
LHA
Day
1
2
Social stress
(or Novel mouse)
+
4OH-Tamoxifen
41-64
Habituation
(fat and cable)
65
Food assay:
Baseline +
Stimulation
J
mPFC
LHA
fiber
f
DMH
VMH
K
Fat intake (Δbsl; kCal)
2.0
1.5
1.0
0.5
0.0
-0.5
*
mPFCNOVEL
mPFCSTRESS